Journal of Hydrology 543 (2016) 686–705

Contents lists available at ScienceDirect

Journal of Hydrology

journal homepage: www.elsevier.com/locate/jhydrol

Research papers

# Multi-objective assessment of three remote sensing vegetation products for streamflow prediction in a conceptual ecohydrological model

Bushra Naseem [a], Hoori Ajami [a,b], Yi Liu [c], Ian Cordery [a], Ashish Sharma [a,*]

[a] School of Civil and Environmental Engineering, University of New South Wales, Sydney, NSW 2052, Australia
[b] Department of Environmental Sciences, University of California Riverside, Riverside, USA
[c] ARC Centre of Excellence for Climate System Science & Climate Change Research Centre, UNSW, Sydney, Australia

ARTICLE INFO

*Article history:*
Received 21 March 2016
Received in revised form 18 September 2016
Accepted 22 October 2016
Available online 22 October 2016
This manuscript was handled by Tim R. McVicar, Editor-in-Chief, with the assistance of Yongqiang Zhang, Associate Editor

*Keywords:*
Gross Primary Productivity (GPP)
Leaf Area Index (LAI)
Vegetation Optical Depth (VOD)
Conceptual dynamic ecohydrological model
Streamflow prediction

ABSTRACT

This study assesses the implications of using three alternate remote sensing vegetation products in the simulation of streamflow using a conceptual ecohydrologic model. Vegetation is represented as a dynamic component in this model which simulates two response variables, streamflow and one of the following three vegetation attributes: Gross Primary Productivity (GPP), Leaf Area Index (LAI) or Vegetation Optical Depth (VOD). Model simulations are performed across 50 catchments with areas ranging between 50 and 1600 km$^2$ in the Murray-Darling Basin in Australia. Moderate Resolution Imaging Spectroradiometer (MODIS) LAI and GPP products, passive microwave observations of VOD and streamflow are used for model calibration and/or validation. Single-objective model calibration based on one of the vegetation products (GPP, LAI and VOD) shows that GPP is the best vegetation simulating product. On the contrary, LAI produces the best streamflow during validation when the optimized parameters are applied for streamflow estimation. To obtain the best compromise solution for simultaneous simulation of streamflow and a vegetation product, a multi-objective optimization is applied on GPP and streamflow, VOD and streamflow and LAI and streamflow. Results show that LAI and then VOD are the two best products in simulating streamflow across these catchments. Improved simulation of VOD and LAI in a multi-objective setting is partly related to the higher temporal resolution of these datasets and inclusion of processes for converting GPP to net primary productivity and biomass. It is suggested that further development of these remote sensing products at finer spatial and temporal resolutions may lead to improved streamflow prediction, as well as a better simulation capability of the ecohydrological system being modeled.



## 1. Introduction

Ecohydrology seeks to describe the hydrological mechanisms that underlie ecological patterns and processes (Rodriguez-Iturbe, 2000). In recent years, ecohydrology is becoming an active area of research to evaluate the linkages between water resources and ecological processes in different environmental conditions (Newman et al., 2006). During the past years, several ecohydrological models have been developed that characterize various aspects of ecological processes such as soil moisture dynamics and interactions between climate, vegetation and soil (Donohue et al., 2012; Pumo et al., 2008). Therefore, assessment of ecohydrological model simulations is a significant part of model selection and prediction (Kelley et al., 2013). Although many researchers described the vegetation model's predictive ability by comparison with ground observational datasets from the field including Leaf Area Index (LAI), Gross Primary Productivity (GPP), Net Ecosystem Production (NEP) and leaf nitrogen (Prentice et al., 2007; Sitch et al., 2003; Woodward and Lomas, 2004), remotely sensed data are widely used for biomass estimation from small experimental sites to global scale analysis (Ediriweera et al., 2014; Jiménez-Muñoz et al., 2009; Niu et al., 2014; Szczypta et al., 2014) and extensively used as observed data to validate the models capability for simulating vegetation dynamics (Istanbulluoglu et al., 2011; Montaldo et al., 2005; Pasquato et al., 2014; Pumo et al., 2008; Zhang et al., 2009). Many other remotely sensed vegetation products including Gross Primary Productivity (GPP), Leaf Area Index (LAI) and Vegetation Continuous Cover (VCC) become more widely used since the launch of the Moderate Resolution Imaging Spectroradiometer (MODIS) in 1999. MODIS products have been used extensively

* Corresponding author at: School of Civil and Environmental Engineering, University of New South Wales, Kensington, NSW 2052, Australia.
*E-mail address:* a.sharma@unsw.edu.au (A. Sharma).

http://dx.doi.org/10.1016/j.jhydrol.2016.10.038
0022-1694/

for establishing their relationship with ground observational datasets of biomass and vegetation indices, and it was found that remotely sensed vegetation products such as GPP, NPP, LAI, NDVI and EVI (Huete et al., 2006; Jin et al., 2014) are suitable for assessment of vegetation coverage (Ardö, 2015; Glenn et al., 2008; Heiskanen, 2006; Jin et al., 2014; Wei, 2010). In addition previous studies have been undertaken to use remotely sensed data for computing evapotranspiration (Zhang et al., 2009; Zhang and Wegehenkel, 2006), evaluating the impacts of vegetation change on streamflow in paired-catchment experiments (Brown et al., 2005; Zhao et al., 2010), assessing vegetation dynamics using ecohydrological models (Istanbulluoglu et al., 2011; Montaldo et al., 2005; Wegehenkel, 2009) and estimating soil moisture dynamics (Liu et al., 2010, 2009). However, streamflow prediction is not adequately discussed in conceptual ecohydrological modeling studies. Most of the ecohydrological models simulate soil moisture and vegetation dynamics (Arnold et al., 2009; Ceccherini and Castelli, 2012; Ceola et al., 2010; Cervarolo et al., 2010; Choler et al., 2010; Gereta et al., 2002; Schymanski et al., 2009) and estimate the rainfall excess runoff (Istanbulluoglu et al., 2011; Montaldo et al., 2005; Pumo et al., 2008; Quevedo and Francés, 2008; Viola et al., 2013). Key research papers for use of remote sensing data are summarised in Table 1, which includes examples where remotely sensed data have been incorporated in ecohydrological modeling in order to: (i) show importance of vegetation indices for improved simulation of biomass/LAI and soil moisture; (ii) calibrate and validate ecohydrological models; and (iii) highlight the role of vegetation dynamics for streamflow estimation. Among these studies, only LAI is used to estimate streamflow across different catchments based on aridity, vegetation cover and other climatic factors (Tesemma et al., 2015a, 2015b; Zhang et al., 2009).

Despite this progress, previous studies were not aimed at identifying which remote sensing vegetation product is best suited for assessing outputs of conceptual ecohydrological models, particularly for streamflow prediction at a catchment scale. To address this issue, a verified conceptual ecohydrological model, RR-LAI-II (EcoHydr) that simulates two responses: streamflow and Leaf Area Index (LAI), is used in this work (Naseem et al., 2015). The vegetation is represented as a dynamic component in this model and biomass production depends on soil moisture content (Arora, 2002; Miller et al., 2012). To assess the performance of EcoHydr in simulating GPP and LAI, MODIS 8-day LAI and GPP products are used. Apart from these products, we also use the passive microwave based product, Vegetation Optical Depth (VOD) (Liu et al., 2013) as an observed data to assess green leaf production in the model. VOD is an indicator of the water content of both woody and leaf components in terrestrial aboveground vegetation biomass (Liu et al., 2013).

The main aim of our study is to assess the use of three remote sensing vegetation products for ecohydrologic model calibration, and to evaluate resulting improvement in streamflow prediction. Specifically, our objectives are (1) to identify which vegetation product can be better simulated by a conceptual ecohydological model in catchments located across different climatic zones, (2) to explore the impact of model calibration using a vegetation product on streamflow prediction, and (3) to identify the best vegetation product for simultaneous optimization of streamflow and vegetation dynamics using a ecohydrological model.

## 2. Study area and data sources

### 2.1. Study area

On the basis of availability of time series of daily rainfall, potential evapotranspiration (PET) and gauged streamflow data, 50 catchments are selected (Fig. 1a) across the Murray Darling Basin (MDB), Australia (Table 2). The soil type data is from the Digital Atlas of Australian Soils, Department of Agriculture, Australian Bureau of Agricultural and Resource Economics and Science (http://data.daff.gov.au/anrdl/metadata_files/) and is used for parameterization of soil parameters in the EcoHydr model (Fig. 1b). The climate zones are identified using the aridity index (Middleton and Thomas, 1997). These catchments are classified as arid with aridity index values between 0.05 and 0.20, semi-arid (0.20–0.50), sub-humid (0.50–0.65) and humid (>0.65) zones (Fig. 1c). Out of 50 catchments, 8 catchments are in the humid zone, 14 catchments are in the sub-humid zone and the rest of 28 catchments belong to the semi-arid zone. The catchment sizes range from 50 to 1600 km$^2$ and Eucalypts are the dominant vegetation type (https://www.data.gov.au/dataset/vegetation-post-european-settlement-1988) in the selected catchments (Fig. 1d, Table 2). The catchment averaged daily rainfall is from the 5 km $\times$ 5 km gridded daily rainfall of the Australian Water Availability Project (AWAP) database (Raupach et al., 2009).

Some of the study catchments are located in high-elevation parts of the Murray-Darling basin where precipitation is mainly snow during the winter season. To identify these catchments, MODIS /Aqua monthly snow cover product (MYD10CM – version 6) level-3 at 5 km $\times$ 5 km spatial resolution in Climate Modeling Grid (CMG) cells is downloaded from http://nsidc.org/data/MYD10CM. The mean snow coverage (%) is calculated over South-East Australia using 13 years (2003–2015) of data for the duration of June-August (winter season). Only four humid catchments (station ID: 401210, 401216, 405231, 405241) and 2 large catchments (station ID: 405219 and 405227) have mean snow coverage of 10–20%. In latter case, only some parts of the catchment ever have snow cover. Physically based form of daily PET data (Donohue et al., 2009, 2010) based on Penman formulation is downloaded from CSIRO website (https://data.csiro.au/dap/landingpage?execution=e1s2&_eventId=viewDescription) (McVicar et al., 2012). Linear interpolation is applied for missing records of PET data. Eleven years of rainfall, runoff and PET data from 2000 to 2010 are used for model simulations which coincides with the availability of MODIS data products.

### 2.2. Satellite based vegetation datasets

The purpose of using vegetation indices was to assess performance of the EcoHydr model (RR-LAI-II) using remote sensing vegetation products. Our primary focus was to choose products that are directly simulated by the model such as LAI and GPP. MODIS GPP is used to evaluate the model's performance for biomass production and capturing seasonal dynamics of vegetation productivity at a large catchment scale (studied catchments areas ranges from 50 km$^2$ to 1600 km$^2$). The choice of VOD data was based on two reasons: (1) VOD is a Microwave based remote sensing product that is mainly sensitive to water content in aboveground vegetation biomass, including canopy and woody components (Jones et al., 2011; Liu et al., 2015; Andela et al., 2013). As Eucalypts is the dominant vegetation type in the study catchments, VOD is selected for ecohydrologic model calibration. (2) Despite the coarse spatial resolution, VOD has the highest temporal resolution compared to the MODIS products (daily vs 8-day) and long term time series of VOD product is available (Liu et al., 2013, 2015).

NDVI, a widely used vegetation index, was not used in this study as it is a strong indicator of high vegetation cover. While the Enhanced Vegetation Index (EVI) product is sensitive to high biomass, its temporal resolution is every 16 days and it is not used in our analysis.

The satellite derived remote sensing vegetation products used in this study (GPP, LAI and VOD) are independent of each other

**Table 1**
Summary of relevant research conducted in ecohydrological modeling (the current paper is added for completeness). All these studies do no perform comparison of remote sensing vegetation products for better simulation, selection of vegetation indices for streamflow prediction and simultaneous optimization of two response outputs from an ecohydrological model and these are denoted with a N/A 'not applicable' in the column of 'Key results'. In the 'Key results' column the abovementioned three components are identified by the code: (1) simulation of remote sensing vegetation products in ecohydrological modeling; (2) significance of remote sensing datasets to improve streamflow estimation and (3) relationship of streamflow with vegetation cover or impact of vegetation indices on the water balance of the catchments.

| Study | Data/model used | Location/study size | Key results |
|---|---|---|---|
| Zhang et al. (2009) | LAI/SIMHYD | South East Australia, 120 catchments | 1. N/A<br>2. The use of remotely sensed evapotranspiration data for model calibration and the use of MODIS LAI data as inputs to a modified SIMHYD model can improve the modeling of daily and monthly runoff series in ungauged catchments<br>3. comparison of the modeling results using daily LAI time series with a constant mean LAI value as input for the entire simulation in regionalization results indicate that the modeled runoff with daily LAI series are better (higher NSE values) than the modeled runoff with a constant LAI value |
| Yang et al. (2009) | NDVI-AVHRR/Budyko hypothesis | China 62 catchments (Yellow River basin), 30 catchments (Hai River basin), and 7 catchments (Inland River basin) | 1. N/A<br>2. The NDVI data is used to compute the fraction of the green vegetation in the region. Incorporation of NDVI data in regional water balance model improves the estimation of the interannual variability of evapotranspiration<br>3. Estimation of the inter-annual variability of regional water balance can be improved by considering the inter-annual variability of vegetation coverage |
| Zhao et al. (2010) | Climate data/Paired-catchment experiment | Australia, *Southwest Western Australia*,, *Tumut in New South Wales* Melbourne, Stewarts Creek, New Zealand (Glendhu catchment and South Africa, *Cathedral Peak* | 1. N/A<br>2. N/A<br>3. The time trend analysis method, and the sensitivity based Approach (to calculate the effect of climate variability on streamflow) provided similar estimates of changes in streamflow because of vegetation effects. Climate and vegetation are the dominant drivers for streamflow change |
| Li and Ishidaira (2012) | LAI, NPP/HYMOD-LPJ GUESS | Angat at Manila-Philippines, Haji at Hiroshima-Japan, Yangtze at Hushan-China, Todd at Alice Springs Australia | 1. The LPJH can simulate vegetation biomass reasonably well in humid basins. LAI simulation is validated using NDVI data. Leaf Area index (LAI) and fraction plant cover (FPC) were simulated and compared with NDVI and with observed data from Japan Integrated Biodiversity Information System (J-IBIS) for the Haji basin in Japan<br>2. 3. Coupled model LPJH (HYMOD and LPJ-GUESS) improves streamflow predictions as compared to the standalone hydrological model, HYMOD |
| Istanbulluoglu et al. (2011) | LAI/Bucket Grassland Model (BGM) | Nebraska Sand Hills (NSH), USA | 1. LAI is simulated from an ecohydrological model and vegetation dynamics is well-captured through simulation<br>2. MODIS LAI is used as observed data for comparison with field data of LAI. In comparison, MODIS-LAI is usually consistent with the field-derived LAI, but appears to be slightly higher in 2 years and shows earlier onset of growth<br>3. N/A |
| Xu et al. (2012) | fPAR data - AVHRR/climate elasticity model | South-east Australia/193 catchments | 1. N/A<br>2. N/A<br>3. Annual runoff, evapotranspiration and runoff coefficient increase with increases in vegetation cover |
| Van Dijk et al. (2013) | VOD/NDVI/conceptual model based on Budyko's theory and process based model AWRA-L | Australia | 1. NDVI is simulated using AWRA model and the model NDVI was calibrated for MODIS NDVI (2000 onward), the model estimated NDVI reduced over time due to reduced rainfall<br>2. VOD and NDVI are used for assessment of agricultural droughts<br>3. Change in magnitude of soil moisture, streamflow, and groundwater is observed due to agricultural and ecological droughts |
| Ediriweera et al. (2014) | LIDAR/Landsat TM images/ Regression Analysis | North-eastern Australia (Richmond Range National Park, the Border Ranges National Park, New South Wales) | 1. 1.N/A<br>2. Improving predicting capacity of plot-scale above-ground biomass (AGB) estimation by fusion of LiDAR and Landsat5 TM derived biophysical variables<br>3. N/A |
| Niu et al. (2014) | LIDAR DEM, MODIS LAI/CATHY NoahMP ecohydrological model | Southeastern Arizona, USA | 1. LAI, surface water and $CO_2$ fluxes simulated quite well over the entire catchment.<br>2. MODIS LAI is used as observed data for comparison with observed net CO2 fluxes.<br>3. N/A |

**Table 1** (*continued*)

| Study | Data/model used | Location/study size | Key results |
|---|---|---|---|
| Pasquato et al. (2014) | EVI, LAI/WUE and LUE models | Valdeinfierno catchment, Spain | 1. N/A<br>2. MODIS products (LAI, EVI) are used to identify the best vegetation indices for verification of conceptual? ecohydrological models<br>3. N/A |
| Tesemma et al. (2015a) | Global Land Surface Satellite (GLASS) LAI data/variable infiltration capacity (VIC) hydrological model | Goulburn–Broken catchment, Australia | 1. N/A<br>2. Satellite derived LAI data is used to improve streamflow prediction.<br>3. LAI is incorporated into a hydrological model to estimate changes in mean monthly and annual runoff. Changes in leaf area index (LAI) with the variable infiltration capacity (VIC) hydrological model are estimated to improve catchment streamflow prediction under a changing climate. |
| Tesemma et al. (2015b) | Global Land Surface Satellite (GLASS) LAI data/variable infiltration capacity (VIC) hydrological model | Goulburn–Broken catchment, Australia | 1. N/A<br>2. VIC was calibrated with both observed monthly LAI and long-term mean monthly LAI (input), derived from the Global Land Surface Satellite (GLASS) leaf area index dataset<br>3. By including the year-to-year variability of LAI in the model, overestimation or underestimation of runoff during wet and dry periods was observed, thus reflecting the responses of vegetation to fluctuations in climate |
| Ruiz-Pérez et al. (2016) | LAI/LUE model/Biome-BGC model | Forest Monte de la Hunde y Palomeras, Spain/ Experimental plot | 1. LAI is simulated<br>2. A parsimonious model is used to simulate vegetation (LAI) and hydrological dynamics (soil moisture), using both field measurements and satellite data in calibration and validation of the model<br>3. N/A |
| This study | GPP,VOD and LAI data/EcoHydr (merged ecohydrological model) | Murray-Darling basin, South East Australia/50 catchments (50–1600 km$^2$) | 1. Calibration and validation of three remote sensing vegetation products GPP, VOD and LAI shows that GPP is the best simulating vegetation product for vegetation simulation in ecohydrological modeling<br>2. The simulations of remote sensing vegetation products GPP, VOD and LAI are compared to assess the impact of vegetation for streamflow prediction<br>3. LAI is identified as the best satellite derived vegetation product to be a part of a conceptual ecohydrological model for better streamflow prediction using multi-objective algorithm |

and are processed from different sensors using different algorithms. The TIMESAT software package (Jönsson and Eklundh, 2004) was used to smooth the time series data of MODIS LAI and GPP. The Savitzky–Golay filtering method was applied to exclude extremes and outliers. To remove the noise from the VOD dataset, a 29-day moving average window on the daily VOD time series was applied (Liu et al., 2011). The detail of each product is given below.

*Leaf Area Index:* LAI is the total one-sided area of leaf tissue per unit ground surface area (Bréda, 2003). The level-4 MODIS global LAI (MODIS15A2, collection 5) product was acquired from the Land Processes Distributed Active Archive Centre (LP DAAC, http://lpdaa.usgs.gov) for the period of February 2000–2010. The LAI data is composited every 8 days and has a spatial resolution of one kilometre. LAI data is retrieved from the land cover classification that is compatible with the radiative transfer model used in their derivation. The land cover classification is based on vegetation structure and is derived from the MODIS land cover product. Therefore, the algorithm has interfaces with the MODIS surface reflectance product (MOD09) and the MODIS Land Cover Product (MOD12) (Knyazikhin et al., 1998).

*Gross Primary Productivity:* The Terra/MODIS Gross Primary Productivity (GPP) product (MOD17A2, collection 5) is an 8-day composite at 1-km spatial resolution delivered as a gridded level-4 product in Sinusoidal projection (LP DAAC, http://lpdaa.usgs.gov). The algorithm for GPP estimation is based on the radiation conversion efficiency parameter. This parameter converts Absorbed Photosynthetically Active Radiation (APAR) to NPP and shows tissue growth or biomass. The APAR is derived from the satellite-derived Fraction of Photosynthetically Active Radiation (FPAR) (from MOD15) and independent estimates of Photosynthetically Active Radiation (PAR) (APAR = PAR $*$ FPAR). Measures of absorbed photosynthetically active radiation (APAR) integrate the geographic and seasonal variability of day length and potential incident radiation with daily cloud cover and aerosol attenuation of sunlight. In addition, APAR implicitly quantifies the amount of leafy canopy that is displayed to absorb radiation (Heinsch et al., 2003).

*Vegetation Optical Depth*: The VOD retrieval algorithm, Land Parameter Retrieval Model (LPRM), uses a radiative transfer model to extract soil moisture and VOD simultaneously (Meesters et al., 2005; Owe et al., 2001, 2008). The vegetation is considered a layered semi-transparent medium and VOD is a measure of the vegetation transmissivity. When the VOD equals 0, the corresponding transmissivity is 1, which means that there is no vegetation attenuation on the microwave emission of the soils (i.e., bare soil). The VOD increases with vegetation density. Over densely vegetated areas such as tropical rainforest, the transmissivity gets close to zero and the microwave emissions are dominated by vegetation. VOD is mainly sensitive to water content in aboveground vegetation biomass, including canopy and woody components (Jones et al., 2011; Liu et al., 2015; Andela et al., 2013). Liu et al. (2011) generated a long-term VOD dataset by smoothing and merging the VOD retrievals from the Special Sensor Microwave Imager (SSM/I, September 1987–2007) and the Advanced Microwave

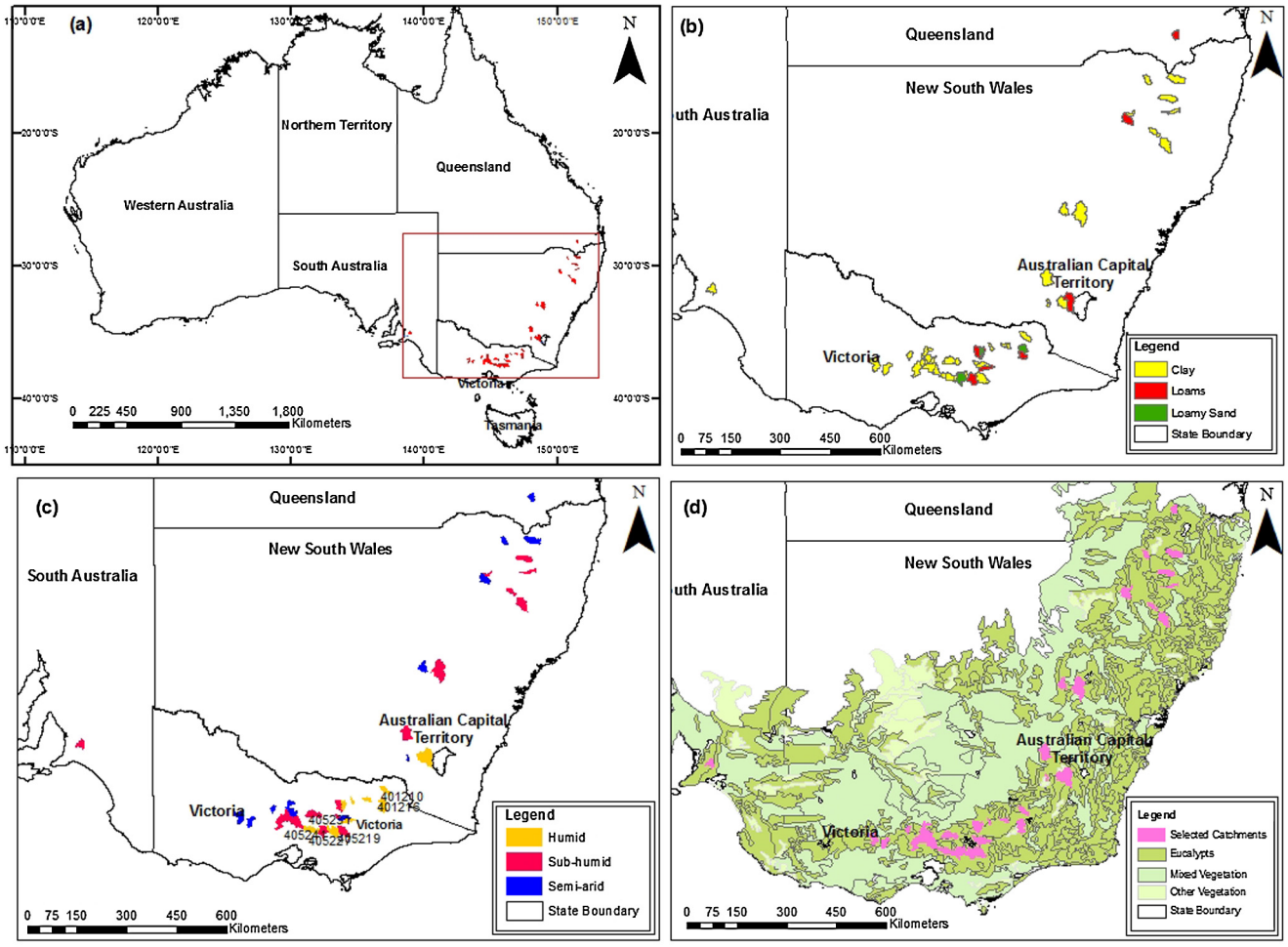


**Fig. 1.** (a) Location of the 50 study catchments in the Murray Darling Basin, Australia; Catchments are classified according to (b) soil type, (c) aridity index and (d) dominant vegetation type. (For interpretation of the references to colour in this figure legend, the reader is referred to the web version of this article.)

Scanning Radiometer (AMSRE, July 2002–September 2011). The smoothed long-term VOD dataset has a 25 km × 25 km spatial resolution and daily temporal interval, and can capture the seasonal dynamics and long-term changes in total aboveground vegetation water content and biomass over various land cover types globally (Liu et al., 2013).

## 3. Methodology

A conceptual ecohydrological model, EcoHydr is first calibrated and validated using three remote sensing observations in a single objective calibration framework. Later the simultaneous calibration of the model with streamflow and each of the remote sensing products is explored. During model calibration response outputs for a given set of assumed conditions are compared with observations and model parameter values are adjusted to achieve a better fit. Model validation involves running a model using parameters that were determined during the calibration, and comparing the predictions to the observed data that are not used in the calibration (Arnold et al., 2012).

The Shuffled Complex Evolution (SCE-UA) algorithm (Duan et al., 1992, 1993) is used to calibrate the EcoHydr model for a single output (GPP, VOD and LAI). The multi-objective complex evolution (MOCOM-UA) (Yapo et al., 1998) algorithm is used to calibrate the model for streamflow and one of the vegetation products, i-e GPP (VOD and LAI). The multi-objective calibration is associated with finding the solutions in which a set of objective functions are simultaneously minimized or maximized depending on the objective function (Yapo et al., 1998). In a multi-objective optimization, there is no single optimal solution and the interaction among different objective functions gives rise to a set of compromised solutions, largely known as the trade-off, nondominated, non-inferior or Parteo solutions. The common purpose of a multi-objective optimization is to choose the best trade-offs among all defined objective functions (Savic, 2002).

The split sampling technique was applied to the available observations to reduce the impact of local optima on model calibration. The split sampling technique basically splits available observations into two sampling periods. One sample is used to calibrate the model and the other one is used to test model predictions using calibrated parameter sets from the calibration period (Mourad et al., 2005). In this study, 11 years of data are split in two periods of 5 years length referred to as scenario 1 and 2 in Table 3. The calibration and validation periods are of 5 years for GPP, LAI and VOD. Year 2000 and 2005 are the warm up period for scenario 1 and 2 respectively to reduce the impact of initial conditions. All 50 catchments are calibrated for scenario 1 and 2 demonstrated in Table 2 individually.

Apart from the split sampling calibration and validation, the nearest neighbour regionalization is also performed to test the model performance and assess the benefits of using remote sensing data for model calibration. A classic regionalisation method based on spatial proximity is used, where the closest catchment to each of the 50 studied catchments calibrated for scenario 1 and 2 is

**Table 2**
Characteristics of the 50 catchments within the Murray-Darling basin, including mean annual rainfall, potential evapotranspiration (PET), runoff, soil and vegetation types and aridity class.

| | Station ID | Area ($km^2$) | Mean annual rainfall (mm) | Mean annual PET (mm) | Mean annual runoff (mm) | Vegetation type | Soil type | Aridity class |
|---|---|---|---|---|---|---|---|---|
| 1 | 401210 | 407 | 1262 | 1475 | 360 | Eucalypts | Loamy sand | Humid |
| 2 | 401216 | 366 | 1450 | 1317 | 428 | Eucalypts | Loams | Humid |
| 3 | 401220 | 459 | 1011 | 1555 | 237 | Eucalypts | Clay | Sub-humid |
| 4 | 402206 | 126 | 1152 | 1542 | 156 | Eucalypts | Clay | Humid |
| 5 | 403213 | 229 | 930 | 1528 | 159 | Eucalypts | Loamy sand | Sub-humid |
| 6 | 403214 | 135 | 1057 | 1569 | 103 | Eucalypts | Clay | Sub-humid |
| 7 | 403224 | 155 | 884 | 1603 | 122 | Eucalypts | Clay | Sub-humid |
| 8 | 403226 | 108 | 920 | 1567 | 122 | Eucalypts | Loams | Sub-humid |
| 9 | 404207 | 456 | 852 | 1536 | 570 | Eucalypts | Loams | Sub-humid |
| 10 | 405205 | 108 | 1166 | 1433 | 334 | Eucalypts | Clay | Humid |
| 11 | 405209 | 619 | 1203 | 1419 | 348 | Eucalypts | Loamy sand | Humid |
| 12 | 405212 | 336 | 696 | 1523 | 348 | Eucalypts | Clay | Semi-arid |
| 13 | 405214 | 368 | 934 | 1476 | 198 | Eucalypts | Clay | Sub-humid |
| 14 | 405215 | 374 | 1041 | 1443 | 198 | Eucalypts | Loams | Sub-humid |
| 15 | 405217 | 363 | 966 | 1450 | 360 | Eucalypts | Clay | Sub-humid |
| 16 | 405219 | 694 | 1101 | 1478 | 364 | Eucalypts | Clay | Humid |
| 17 | 405227 | 632 | 1208 | 1463 | 364 | Eucalypts | Loams | Humid |
| 18 | 405228 | 471 | 693 | 1502 | 78 | Eucalypts | Clay | Semi-arid |
| 19 | 405229 | 108 | 485 | 1630 | 15 | Eucalypts & others | Clay | Semi-arid |
| 20 | 405230 | 253 | 499 | 1619 | 15 | Eucalypts & others | Clay | Semi-arid |
| 21 | 405231 | 187 | 896 | 1476 | 11 | Eucalypts | Clay | Sub-humid |
| 22 | 405240 | 612 | 638 | 1523 | 52 | Eucalypts | Clay | Semi-arid |
| 23 | 405241 | 129 | 1286 | 1351 | 46 | Eucalypts | Clay | Humid |
| 24 | 405245 | 119 | 773 | 1497 | 660 | Eucalypts | Clay | Sub-humid |
| 25 | 405248 | 290 | 552 | 1618 | 119 | Eucalypts | Clay | Semi-arid |
| 26 | 405274 | 191 | 681 | 1516 | 393 | Eucalypts | Clay | Semi-arid |
| 27 | 405291 | 52 | 647 | 1532 | 67 | Eucalypts | Clay | Semi-arid |
| 28 | 405293 | 179 | 556 | 1606 | 23 | Eucalypts | Clay | Semi-arid |
| 29 | 406213 | 629 | 693 | 1500 | 47 | Eucalypts | Clay | Semi-arid |
| 30 | 406214 | 234 | 549 | 1637 | 21 | Eucalypts | Clay | Semi-arid |
| 31 | 406226 | 175 | 585 | 1573 | 9 | Eucalypts | Clay | Semi-arid |
| 32 | 406235 | 214 | 633 | 1532 | 30 | Eucalypts | Clay | Semi-arid |
| 33 | 407213 | 470 | 523 | 1574 | 11 | Eucalypts & others | Clay | Semi-arid |
| 34 | 408206 | 675 | 525 | 1577 | 18 | Eucalypts & others | Clay | Semi-arid |
| 35 | 410024 | 990 | 1017 | 1517 | 11 | Eucalypts | Loams | Sub-humid |
| 36 | 410044 | 1025 | 574 | 1697 | 16 | Eucalypts & others | Clay | Semi-arid |
| 37 | 410057 | 673 | 1026 | 1558 | 267 | Eucalypts & others | Clay | Sub-humid |
| 38 | 410061 | 155 | 942 | 1557 | 136 | Eucalypts & others | Clay | Sub-humid |
| 39 | 416008 | 866 | 737 | 1825 | 19 | Eucalypts & others | Clay | Semi-arid |
| 40 | 416016 | 761 | 823 | 1771 | 53 | Eucalypts | Clay | Semi-arid |
| 41 | 416020 | 402 | 689 | 2003 | 52 | Eucalypts | Clay | Semi-arid |
| 42 | 418021 | 311 | 807 | 1673 | 24 | Eucalypts | Clay | Semi-arid |
| 43 | 418027 | 220 | 820 | 1934 | 100 | Eucalypts | Clay | Semi-arid |
| 44 | 419016 | 893 | 795 | 1707 | 55 | Eucalypts & others | Clay | Semi-arid |
| 45 | 419029 | 389 | 734 | 1836 | 18 | Eucalypts | Clay | Semi-arid |
| 46 | 419051 | 663 | 742 | 1959 | 30 | Eucalypts & others | Loams | Semi-arid |
| 47 | 421018 | 1620 | 682 | 1742 | 43 | Eucalypts | Clay | Semi-arid |
| 48 | 421048 | 579 | 606 | 1838 | 18 | Eucalypts & others | Clay | Semi-arid |
| 49 | 422338 | 396 | 594 | 1982 | 69 | Eucalypts | Loams | Semi-arid |
| 50 | 426533 | 470 | 650 | 1627 | 56 | Eucalypts | Clay | Semi-arid |

identified. Next, the calibrated parameter set from the donor catchment is used to simulate streamflow and LAI, GPP and VOD in a catchment that is geographically closest to the calibrated donor catchment. This regionalization approach for model validation was also applied for the two scenarios (2001–2005 and 2006–2010) given in Table 3.

### 3.1. Designing simulation experiments

To evaluate the performance of the conceptual ecohydrological model, EcoHydr, for vegetation product simulations, single-objective optimization is performed on catchment averaged observational data of GPP, LAI and VOD using the Shuffled Complex Evolution (SCE-UA) algorithm (Duan et al., 1992, 1993). The objective of this individual and independent calibration was to identify which remote sensing product is better simulated by a conceptual ecohydrologic model. A single-objective calibration consists of determining the set of model parameters that optimizes (maximizing or minimizing) a single-objective function. Objective functions express the agreement between observed and simulated catchment behaviour in a numerical form (Fenicia et al., 2007). The Nash-Sutcliffe Efficiency (NSE) (Nash and Sutcliffe, 1970) was used as the evaluation performance criterion (objective function) for vegetation product simulations. For simplicity, objective functions

**Table 3**
Calibration and validation time periods for model evaluation.

| Scenario | Warm up year | Calibration period | Years | Warm up year | Validation period | Years |
|---|---|---|---|---|---|---|
| 1 | 2000 | 2001–2005 | 5 | 2005 | 2006–2010 | 5 |
| 2 | 2005 | 2006–2010 | 5 | 2001 | 2001–2005 | 5 |

that are explicitly designed for use in ephemeral catchments which are common in Australia (Smith et al., 2010) have not been considered. Future work will attempt to repeat the analysis with consideration for the uncertainty in model simulations, using a data-defined likelihood framework (Smith et al., 2015) rather than the objective functions used here (Naseem et al., 2015).

Three validation tests are performed for the single-objective optimization experiments of EcoHydr using vegetation products.

(a) First, a calibrated parameter set for each vegetation product (e.g. GPP) is used to validate the EcoHydr performance for that particular product (e.g. GPP).
(b) Second, the nearest neighbour regionalization, a classic regionalisation method based on spatial proximity is used. In this approach, the calibrated parameter set from a donor catchment is used to simulate the vegetation product in the geographically closest catchment.
(c) Third, the validation was performed against daily observed streamflow using a calibrated set of parameters from GPP, LAI and VOD calibrations.

To evaluate the best vegetation product to be a part of a conceptual ecohydrological model calibration, the multiobjective complex evolution (MOCOM-UA) algorithm (Yapo et al., 1998) is performed on streamflow and a vegetation product. This approach is considered for three cases of simultaneous optimization as follows:

(a) streamflow and GPP,
(b) streamflow and LAI, and
(c) streamflow and VOD.

The same scenarios described in Table 3 were used for these simultaneous optimizations. The parameter estimation using the multi-objecctive algorithm is based on the NSE of streamflow and NSE of one of the vegetation products i-e MODIS GPP; MODIS LAI and VOD. Following the calibration, the nearest neighbour regionalisation is performed only on streamflow by using one calibrated set of parameters of streamflow obtained through multi-objective algorithm.

### 3.2. Ecohydrological model (EcoHydr)

EcoHydr is a merged ecohydrological model in which rainfall-runoff processes of a lumped hydrologic model, HYMOD (Boyle et al., 2003; Wagener et al., 1999) are merged with the biomass production approach of the Bucket Grassland Model (BGM) (Istanbulluoglu et al., 2011). The rainfall-runoff modeling part of HYMOD uses daily rainfall and PET as input variables and predicts ET and streamflow. HYMOD has 7 parameters that are estimated by calibration (Table 4). The simple structure of this model includes a non-linear soil moisture storage tank to simulate rainfall excess runoff along with two series of linear tanks to simulate the slow-flow and quick flow components of runoff. Fig. 2 of the model illustrates that $C_{max}$ is the maximum soil moisture capacity within the catchment and C(t) is the soil moisture storage at time t. The amount of precipitation that exceeds $C_{max}$ flows through linear quick flow and slow flow tanks using the fraction coefficient $\alpha$. The slow flow tanks represent the subsurface storage. The total streamflow of the catchment is the summation of discharge from the quick and slow flow tanks. All model equations are presented in the appendix.

A separate part of the model is based on dynamic vegetation modeling that computes above ground green and dead biomass based on net primary productivity and water use efficiency in response to soil moisture dynamics (Fig. 2) (Istanbulluoglu et al., 2011; Williams and Albertson, 2005). In addition, Gross Primary Productivity (GPP) is calculated on the basis of water use efficiency (WUE) parameter (WUE, kg $CO_2$ kg $^{-1}$ $H_2O$) that srepresents the amount of carbon gained for each unit of water lost (Williams and Albertson, 2005).and actual evapotranspiration (Eq. (5)–Appendix). From GPP, NPP is estimated using equation 6 of the Appendix. LAI is calculated by multiplying simulated leaf biomass by the specific leaf area (SLA, $m^2$ leaf $g^{-1}$ DM) (Fig. 2(II) and Table 5). The state variables of this model include green biomass [Bg, kg DM $m^{-2}$], dead biomass [Bd, kg DM $m^{-2}$] and vegetation cover fraction (Vt). RR-LAI-II (EcoHydr) model is selected in this study as it performed well for simulating streamflow and LAI in an earlier study focussed on comparison of two conceptual ecohydrologic models with a simple rainfall-runoff model in the same study region (Naseem et al., 2015). The simulations are performed with a daily time step and equations are solved using the Euler's approximation scheme (Butcher, 2008).

The EcoHydr model is calibrated independently for four cases of 8-day GPP, 8-day LAI, daily VOD (Fig. 2a (I, II & III)) and 8-day VOD. Performing the calibration test for VOD on a 8-day time step provides a fair comparison with other vegetation products and removes the impact of temporal resolution of the observed data on calibration and comparison among multiple products. Observed VOD is sensitive to dynamics of water content in total aboveground biomass (including green and non-green biomass). Here we first convert the simulated green biomass from the model to $VOD_{GREEN}$ by introducing a proportionality parameter (Eq. (11) Appendix). Our assumption is that green biomass is linearly related to water content in the green component of Eucalypt forests, and therefore the $VOD_{GREEN}$ is comparable to the satellite derived VOD with the assumption that the observed VOD dynamics are mainly from the green components of Eucalypt forests. All seven parameters of the hydrological model (Table 4) are optimized for every case (GPP, LAI and VOD). For the ecological part, three parameters are optimized for LAI and GPP, and four parameters for the VOD simulations in addition to the seven hydrologic parameters. As a proportionality parameter is introduced for biomass conversion to VOD, simulations based on VOD have one additional parameter (Table 4).

## 4. Results

To test the model's robustness and capability in reproducing the satellite-derived vegetation dynamics, three cases were considered: (1) single-objective calibration and validation of EcoHydr using each product (GPP, LAI and VOD), (2) validation of simulated streamflow from the EcoHyr model using the calibrated parameter sets resulting from calibrating the model using each vegetation product, and, (3) multi-objective calibration and validation of streamflow and GPP, streamflow and VOD and streamflow and LAI.

### 4.1. Single-objective calibration experiment: calibration and validation based on GPP, LAI and VOD

The performance of the EcoHydr model was assessed in terms of its ability to reproduce the observed satellite derived products of GPP, LAI and VOD. The Cumulative Distribution Function (CDF) curves are plotted based on NSE values of both scenarios (Table 3) from 2001 to 2010 for calibration (Fig. 3a) and validation (Fig. 3b). The calibration results of all three remote sensing products show that model's performance for GPP simulation is better than LAI and VOD. The CDF curves of all the satellite-derived products reveal that percentage of scenarios between calibration and validation is significantly different for LAI and VOD compared to GPP. For GPP, almost 35% of scenarios have NSE greater than 0.7 in the calibration period while this percentage remains maintained in the

**Table 4**
Soil parameters description, value ranges and sources for EcoHydr model.

| Parameters | Description | Range | Source |
|---|---|---|---|
| $C_{max}$ [mm] | Maximum Soil storage capacity of a catchment | 300–3000 | Calibrated |
| β [–] | Degree of spatial variability of soil moisture capacity | 0.1–2 | Calibrated |
| α [–] | Partitioning factor between quick and slow flow tanks | 0.1–1 | Calibrated |
| Ks [$day^{-1}$] | Residence time for slow flow tanks | 0.0001–0.1 | Calibrated |
| Kq [$day^{-1}$] | Residence time for quick flow tanks | 0.1–1 | Calibrated |
| Nq | Number of quick flow tanks | 1–3 | Calibrated |
| Ns | Number of slow flow tanks | 1–2 | Calibrated |

Parameters describing soil characteristics of different soil types used in EcoHydr[a]

| | $S_h$ (Saturation degree at soil hygroscopic point) | $S_w$ (Saturation degree at wilting point) | $S^*$ (Saturation degree at stomata closure) | $S_{fc}$ (Saturation degree at Field capacity) |
|---|---|---|---|---|
| Loamy Sand | 0.08 | 0.11 | 0.31 | 0.52 |
| Clay | 0.47 | 0.52 | 0.78 | 0.99 |
| Loams | 0.19 | 0.24 | 0.57 | 0.65 |

[a] Laio et al. (2001).

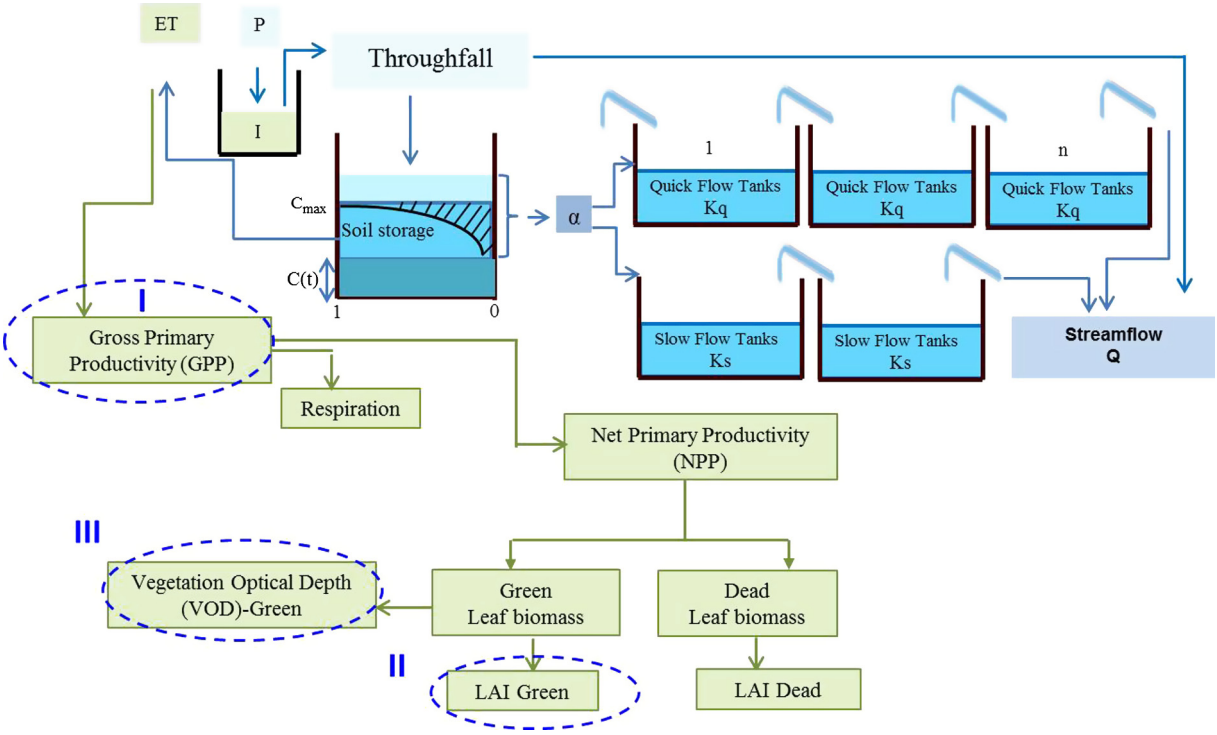


**Fig. 2.** *Blue boxes show hydrological processes, green boxes show vegetation related processes, notations are I: interception, n: numbers of tanks, P: precipitation, ET: evapotranspiration, α, Ks, Kq: parameters (Table 4). Ecohydroloic processes of EcoHydr model (a conceptual ecohydrological model). The model simulates daily ET, streamflow and changes in catchment storage on the basis of daily rainfall and PET. Daily ET is controlled by the soil available water content which subsequently controls gross primary production through the WUE parameter. After taking into account respiration, net primary productivity is partitioned to green and dead leaf biomass.

validation period. The percentage of scenarios with the NSE score of >0.7 is significantly reduced for the VOD and LAI during calibration and validation periods. Only 25% and 15% of scenarios have NSE greater than 0.7 for VOD and LAI in calibration period respectively. This percentage is further reduced in validation for VOD and LAI to only 8%. Similarly, almost 75% of the calibration scenarios have NSE greater than 0.5 for GPP and VOD and 42% for LAI. In validation period, this percentage reduces to 35% for VOD and LAI while percentage of GPP does not change. To evaluate the findings that GPP is the best reproducing product from this ecohydrological model, the CDF curves are drawn separately for all catchments in forward (2006–2010) and backward (2001–2005) time frames during validation period (Fig. 3c and d). It is noticeable that validation of GPP is better than other two remote sensing products: VOD and LAI. NSE values for VOD and LAI is higher in backward time frame as compared to forward time frame. Almost 40% of catchments have NSE greater than 0.6 for GPP in the forward time frame and 70% in the backward time frame. From the results, it is found that GPP is the best simulating product in EcoHydr and the result is independent of the calibration period. There are a number of reasons for these higher NSE values based on GPP. First, GPP is the primary indicator of vegetation carbon fluxes (Sur and Choi, 2013) and has a strong influence on the ecosystem carbon cycle. In our model, GPP is calculated based on water use efficiency (WUE) and actual evapotranspiration (Eq. (5)-Appendix). WUE has a strong dependence on weather condition and leaf phenology (Yu et al., 2008) and for each catchment was assumed to be a constant parameter in EcoHydr using literature values for Eucalypts. There-

**Table 5**
Vegetation parameters description, values, and sources for the EcoHydr model.

| Parameters | Description | Reference key (eucalypts) | Source |
|---|---|---|---|
| $I_{max}$ [mm day$^{-1}$] | Maximum interception | 1.1 | Crockford and Richardson (1990) |
| $k_{sg,}$ [d$^{-1}$] | Natural decay factor for green biomass | | Calibrated |
| $k_{dd}$ [d$^{-1}$] | Natural decay factor for dead biomass | | Calibrated |
| $C_g$ [m$^2$ leaf g$^{-1}$ DM] | Specific leaf area for green biomass | 0.007 | Hunt et al. (2007) and Schulze et al. (2006) |
| $C_d$ [m$^2$ leaf g$^{-1}$ DM] | Specific leaf area for dead biomass | 0.005 | Hunt et al. (2007) and Schulze et al. (2006) |
| WUE [–] | Water use efficiency | 0.016 | Küppers et al. (1992) |
| μ [–] | Ratio of night time to daytime $CO_2$ net ecosystem exchange | 0.3 | Calibrated |
| ẃ [kg DM kg$^{-1}$ $CO_2$] | Conversion of $CO_2$ to dry matter | 0.55 | Istanbulluoglu et al. (2011) |
| $\phi_a$ [–] | Allocation coefficient | 0.81 | Mokany et al. (2006) |
| ParaVOD [–] | Proportionality parameter for converting green biomass to VOD | | Calibrated |

fore, performance of the model is strongly related to simulated actual evapotranspiration which is directly controlled by soil moisture content. Overall, the model is reproducing GPP reasonably well in all catchments. VOD includes both leaf and woody components of biomass that are sensitive to water in the environment and hence provides a measure of above-ground biomass (Liu et al., 2011). There is a gradient in climate, land cover and canopy biomass distribution across VOD patterns (Jones et al., 2011) and its dynamics are estimated globally by Liu et al. (2013) and Andela et al. (2013). VOD takes into account the leaf and woody part of the vegetation as compared to LAI. This is evident from the model's better performance for VOD than LAI in all validation scenarios (Table 3) and catchments in forward and backward time frames. Other possible reasons include that the VOD parameter is a measure of canopy density and vegetation water content, while LAI provides a relative measure of photosynthetic canopy cover. In addition, biophysical differences in the phenology parameters measured by two independent methods for VOD and LAI contribute to the simulation differences (Jones et al., 2011).

To assess the effect of temporal resolution of VOD on EcoHydr's simulations, we resampled the VOD data with an 8 day interval and compared the calibration and validation results across all 50 catchments. No significant differences in NSE are found between calibrating the model with daily and 8-day VOD values (Fig. 4a and b).

In addition to evaluate the spatial and temporal resolution of the data on the performance of the model, we resampled our data at the same temporal interval and spatial resolution for three catchments. All datasets including GPP, VOD and LAI were resampled at 0.05 degree spatial resolution as for meteorological forcing input data and with an 8 day temporal interval (the same as LAI and GPP). The results show that there is no significant change in NSE score in calibration and validation time periods and GPP provides a better simulation of vegetation than VOD and LAI. Spatial resolution and temporal interval of the dataset do not appear to significantly affect the simulation results from our ecohydrological model EcoHydr.

Better simulation of these satellite derived vegetation products depends on a number of ecological factors and how the carbon cycle is parameterized in a dynamic vegetation model. Despite the simple structure of EcoHydr model, its performance is satisfactory particularly for simulating GPP across multiple catchments. However, the response of the ecohydrological model EcoHydr may vary for simulation of the best vegetation product and streamflow depending on the climate and soil type of a catchment.

Apart from model verification using split sampling technique, the results of other validation based on the nearest neighbour regionalization (calibrated parameters are transferred to geographically closest located catchement) are presented in Fig. 5. The results show that EcoHydr produced the best GPP simulations in comparison to VOD and LAI in calibration as shown in (a) and then in validation on spatially located closest catchment for period of year 2001–2005 and 2006–2010 indicated in (c) and (d). The regionalisation results are as good as of the corresponding calibration results. The median NSE is greater than 0.6 in regionalisation of both scenarios in (c) and (d) for GPP while median NSE gets lower for VOD, 0.58 in (g) and 0.45 in (h). This deterioration in NSE regionalisation is persistent in the case of LAI, with median of 0.3 in (k) and 0.29 in (l).

Split sample validation of GPP is as good as for calibration in (b). However, the median NSE becomes lower for VOD (0.5) and LAI (0.35) in (f) and (j) respectively. The regionalisation results suggest that the calibrated parameter values can provide comparable results from the spatial proximity approach.

The catchments are classified according to soil type and aridity index (Fig. 1b and c) to evaluate the model's performance in different soil types and climatic zones. Our results show that the model is consistently performing well for GPP across all climatic zones (Fig. 6a–c) in most of the scenarios and for most of the soil types (Fig. 6d–i). However, the CDF curves of NSE values for all climatic zones show different levels of performance. For example, for the GPP the percentage of scenarios with NSE greater than 0.7 in humid and sub-humid catchments are 40% and 58% respectively and 10% in semi-arid zone. While the percentage of scenarios with NSE greater than 0.7 reduces for VOD inputs, and as for GPP the model is working better in humid zones than semi-arid and sub-humid zones. The performance of the model is lower for LAI compared to GPP and VOD. In the semi-arid zone some higher NSE scores are observed for LAI compared to the humid and sub-humid zones, and 22% of scenarios have negative NSE in semi-arid zones. Poor simulation of LAI in some scenarios is likely related to the vegetation parameterization in the model and perhaps quality of PET data in some catchments. All dynamic vegetation parameterization of the model is based on Eucalypts (Table 5) as Eucalypts are the dominant vegetation type in all the catchments (Fig. 1d). However, other vegetation types and grasses are also present in the studied catchments which must impact the remotely sensed vegetation signal but these effects are not considered in this lumped model.

Apart from the grouping of catchments based on aridity, the CDF curves are also drawn on the basis of aridity and soil type together (Fig. 6d–i). The results reveal that LAI simulations are better in the semi-arid zone with loamy soil types (Fig. 6f) as compared to humid and sub-humid zones with clay and loams. In most of the cases, performance of the model is better for GPP and VOD in humid zones with clay and loams. The performance of the model for better LAI simulation in the semi-arid zone with loamy soil type depends on many factors including landscape heterogeneity, land cover and vegetation type. These attributes are strongly linked with leaf area and soil type (Zhang et al., 2001) and this is evident in our results as shown by the CDF curves.

A direct comparison graph of NSE for individual catchments across different climatic zones is also presented to assess the model performance (Fig. 7). It is found that the model's perfor-

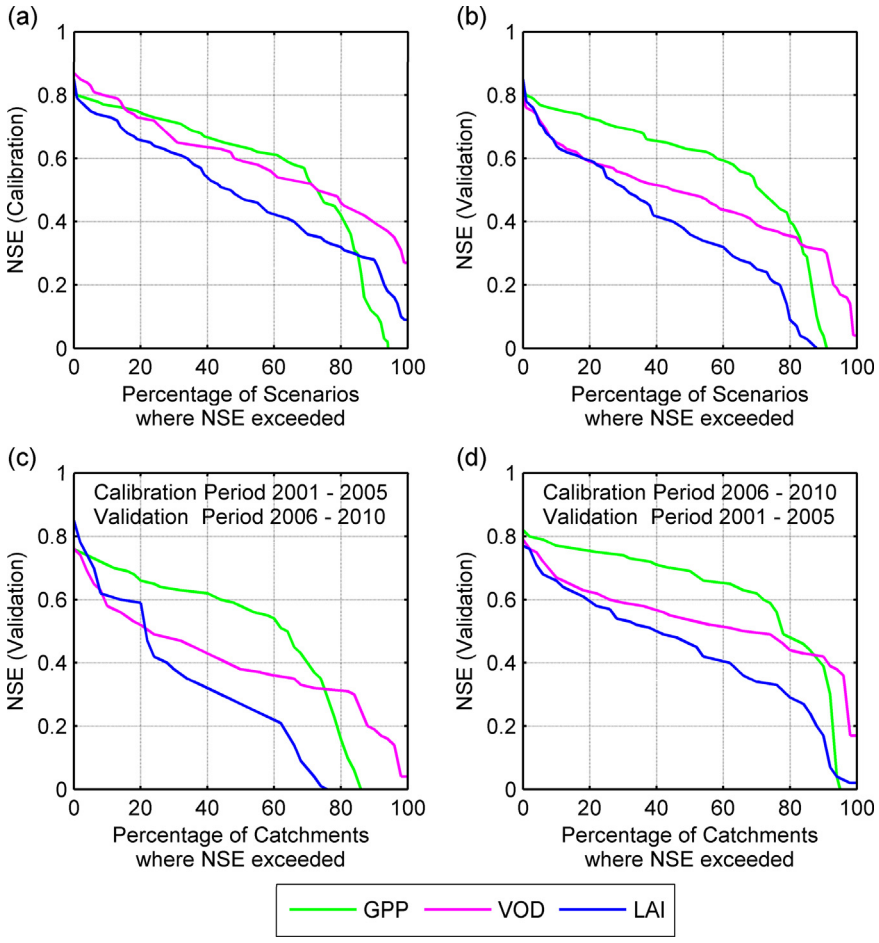


**Fig. 3.** Results of calibration and validation periods of EcoHydr for GPP, VOD and LAI simulation across all the catchments (a) CDF for LAI, VOD and GPP calibration across all scenarios, (b) CDF for LAI, VOD and GPP validation across all scenarios, (c) validation based on forward time frame (2006–2010) across all catchments, (d) validation based on backward time frame (2001–2005) across all catchments. GPP is the best response output among three vegetation remote sensing products shown by higher NSE score as compared to LAI and VOD.

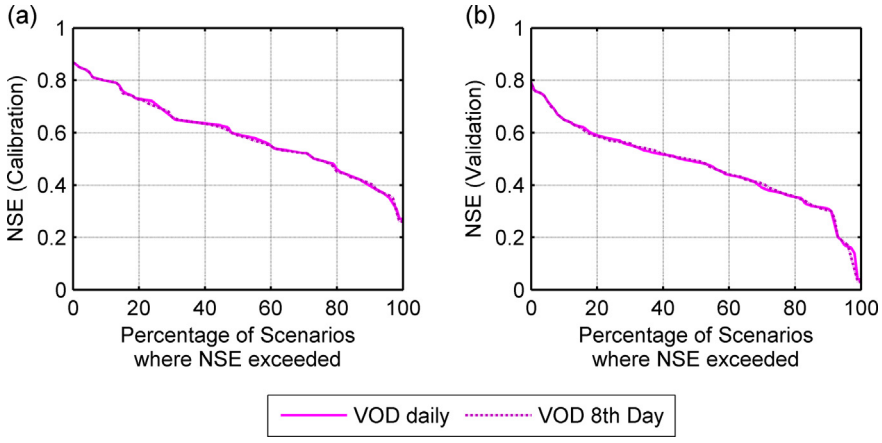


**Fig. 4.** Comparison of daily VOD and 8-day time step.

mance is better in dense forest and humid catchments than semi-arid and sub-humid catchments for the GPP while the performance is not consistent for VOD and LAI. The catchments in our study area vary from 50 to 1600 km$^2$ and have different species of Eucalypts and mixed vegetation. In our conceptual model only the dominant vegetation type is considered to parameterize vegetation dynamics using published parameter values (Table 5) and the impact of catchment heterogeneity is ignored.

To further assess the performance of EcoHydr model, time series of observed and simulated VOD, LAI and GPP for validation scenarios from year 2001–2005 are plotted for three catchments in humid, sub-humid and semi-arid zones (Fig. 8). The seasonal

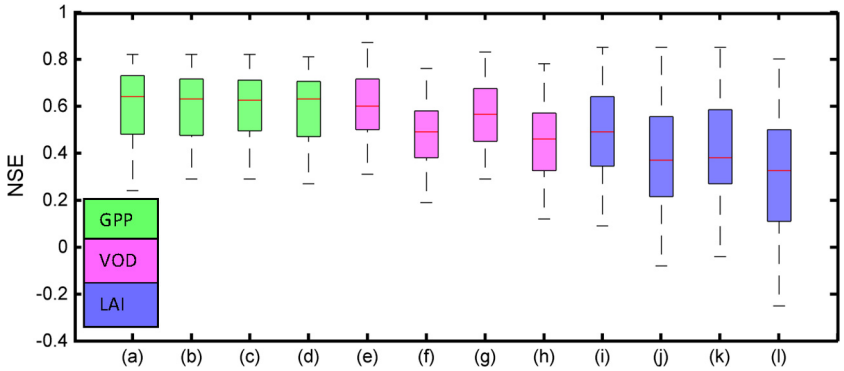


**Fig. 5.** Box plot shows validations of nearest neighbour regionalization approach in comparison to the split sampling technique. Calibration of GPP, VOD and LAI in (a), (e) and (i); validations of same catchments for GPP, VOD and LAI are in (b), (f) and (j), validation on nearest neighbour catchments for scenario 1 (2001–2005) are presented in (c), (g) and (k) for GPP, VOD and LAI and validation on nearest neighbour catchments for scenario 2 (2006–2010) are presented in (d), (h) and (l) for GPP, VOD and LAI.

dynamics of GPP and LAI are well-captured by the model as compared to VOD. In addition, the performance of the model in simulating GPP is equally good across these 3 catchments while LAI simulation is equally good across humid, sub-humid and semi-arid catchments. The performance of the model in simulating VOD for the humid catchment is inferior in comparison with other catchments and GPP. These satellite derived vegetation products show different behaviour towards seasonal vegetation dynamics and there is a signal shift between LAI and VOD as indicated by Jones et al. (2011).

As vegetation processes are an essential part of carbon and water cycles, our conceptual ecohydrological model could capture vegetation dynamics quite well in most of the catchments. In our model, evapotranspiration affects the GPP, NPP, and green biomass production which consequently impacts LAI and VOD dynamics. Moreover, incorporating interception impacts streamflow prediction in EcoHydr model. Despite the simple structure of the model, both vegetation dynamics and catchment scale hydrology are linked with each other which can provide significant insights regarding catchment water balance dynamics and its impact on growth and senescence of vegetation.

### *4.2. Validation of single-objective and multi-objective calibration experiment based on GPP, LAI and VOD on streamflow*

Catchments with diverse climatic conditions, vegetation and soil type can provide useful information about the hydrological role of vegetation in the catchment water balance. The intrinsic coupling of vegetation and water balance is affected by the structure of vegetation, through rainfall interception and transpiration which subsequently impact streamflow (Zhang et al., 2001). Our ecohydrological model EcoHydr computes interception and evapotranspiration and also calculates net primary productivity and vegetation fractional cover both of which strongly depend on evapotranspiration and interception. The structure of the model is a merged type that computes two sets of response outputs, streamflow and the vegetation products LAI, VOD and GPP (Fig. 2). To evaluate our assertion that calibration of vegetation dynamics through LAI, VOD or GPP influences streamflow, we used the calibrated set of parameters (obtained through single-objective calibration of LAI, VOD and GPP) to validate the streamflow observations (Fig. 9a). Our results of validation scenarios show that GPP is producing the best streamflow as compared to VOD and LAI for most of the scenarios while VOD is working better than LAI in most of the cases. Despite better performance of GPP for streamflow prediction compared to LAI and VOD, the percentage of negative streamflow NSE scenarios are higher for GPP (almost 38% of total) as compared to 20% for VOD and LAI (Fig. 9a). The results show the need for a multi-objective calibration as calibrated parameters obtained through calibration based on individual vegetation products do not predict streamflow reasonably well.

Similar to the regionalization approach for the vegetation product simulations, EcoHydr is also validated for streamflow when both response outputs, streamflow and the other vegetation attribute are calibrated simultaneously through a multi-objective algorithm. These parameter sets of donor catchments are used for streamflow prediction in nearest catchments (Fig. 10). The results show that EcoHydr produced the best streamflow predictions based on LAI calibration in comparison to VOD and GPP calibrated models as shown in all the validation scenrarios based on the split sampling scenarios in (b) and (f) and the regionalization approach based on spatially located closest catchment for periods of years 2001–2005 and 2006–2010 indicated in (k) and (l). The regionalisation results for streamflow are as good as of the corresponding calibration results. The median NSE ranges between 0.4 and 0.5 in the regionalisation approach for both scenarios in (k) and (l) for LAI while the median NSE gets lower for VOD (0.3) in (g) and (h). This deterioration in NSE regionalisation is persistent in the case of GPP (NSE ranges between 0.25 and 0.3) in (c) and 0.29 in (d). Split sample validation of streamflow on the same catchments is as good as of calibration period with LAI in (j) while NSE is lower for the other vegetation products, VOD and GPP in (b) and (f). The regionalisation results suggest that the calibrated parameter values can provide comparable results from the spatial proximity approach. Similar to the split sampling approach, LAI is the best vegetation product for streamflow prediction.

### *4.3. Multi-objective calibration experiment*

We also performed three sets of multi-objective optimizations. These were LAI and streamflow, GPP and streamflow and VOD and streamflow. Our results, shown in Fig. 9b indicate that LAI provides the best unique and compromised set of parameters for coherent simulation of streamflow and LAI compared to cases where VOD and GPP are optimized with streamflow (Fig. 9b). A compromised parameter set provides the best possible solution for the combination of two response outputs, streamflow and LAI as evidenced in Fig. 9b. The CDF curves show that 10% of scenarios have NSE greater than 0.8 when LAI is calibrated with streamflow. Same percentage is observed for VOD and none of the scenario reaches to NSE of 0.8 when GPP is calibrated with streamflow. Similarly, the percentage of scenarios with NSE score greater than 0.7 is similar for LAI and VOD (30%) compared to GPP (10%). Almost 40% of scenarios have NSE greater than 0.6 when LAI and VOD are the

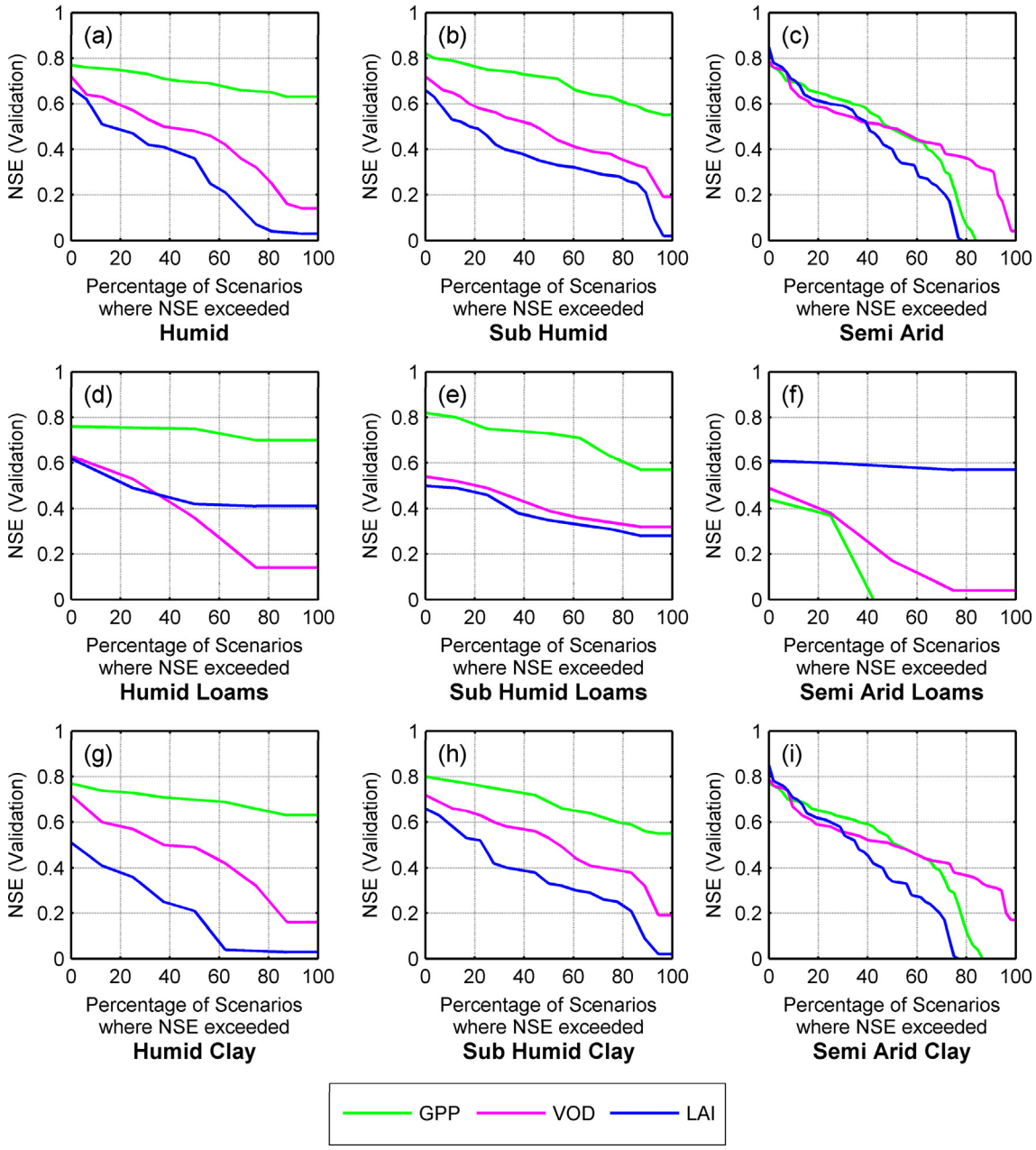


**Fig. 6.** Performance of EcoHydr in validation time frames across all scenarios in catchments located in different climatic zones as well as groupings based on climate and soil type. Higher NSE score is shown for GPP in most of the scenarios as compared to VOD and LAI.

response outputs while this percentage is only 18% when GPP was optimized with streamflow. VOD is the strong indicator of vegetation water content while GPP indicates the rate at which carbon dioxide converts into organic matter. The better percentage of streamflow prediction with VOD rather than with GPP using the multi-objective algorithm can be interpreted as due to inherent differences in these datasets and subtle model structure.

### *4.4. Cross validation of single- and multi-objective experiments for vegetation simulation*

A further assessment was made of applying calibration parameters obtained with one vegetation attribute to determine how these parameters might influence the output when other attributes were modeled. Hence we tried validation of single-objective and multi-objective calibrated parameters of VOD on GPP and LAI, GPP on LAI and LAI parameters on GPP (Fig. 11a and b). In another words, we assessed the performance of the model for the vegetation attribute which is not calibrated through single or multi-objective calibration. Cross validation of single-objective optimization results illustrate that single-objective calibration based on either LAI or VOD results in a different distribution of NSE scores based on GPP. Further, the multi-objective algorithm has higher GPP based NSE scores for the parameters of VOD-streamflow and LAI-streamflow calibration compared to single objective calibration of VOD or LAI. In addition, the percentages of scenarios with negative NSE (based on GPP) became higher in the single-objective calibrations. Single-objective calibrations based on GPP or VOD cause poor simulation of LAI particularly when the model is calibrated based on GPP compared to VOD. Similar to GPP, higher NSE values are obtained for LAI in a multi-objective calibration. The results indicate the significance and

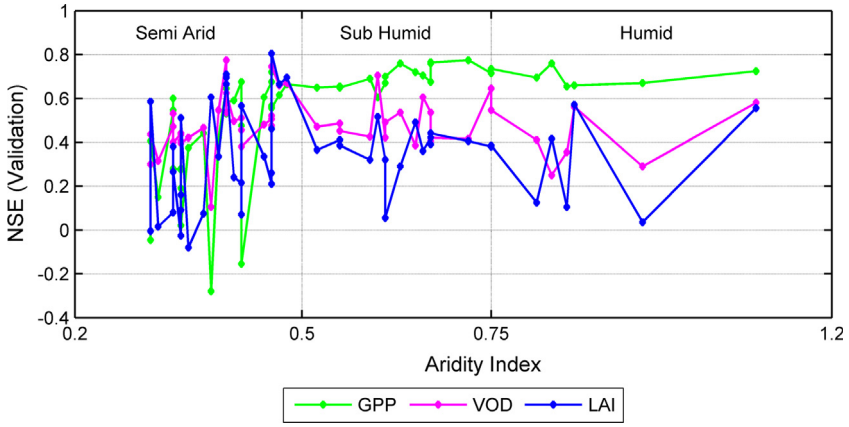


**Fig. 7.** Comparison of mean NSE values (VOD, LAI and GPP) of validation period across individual catchments located in different climatic zones.

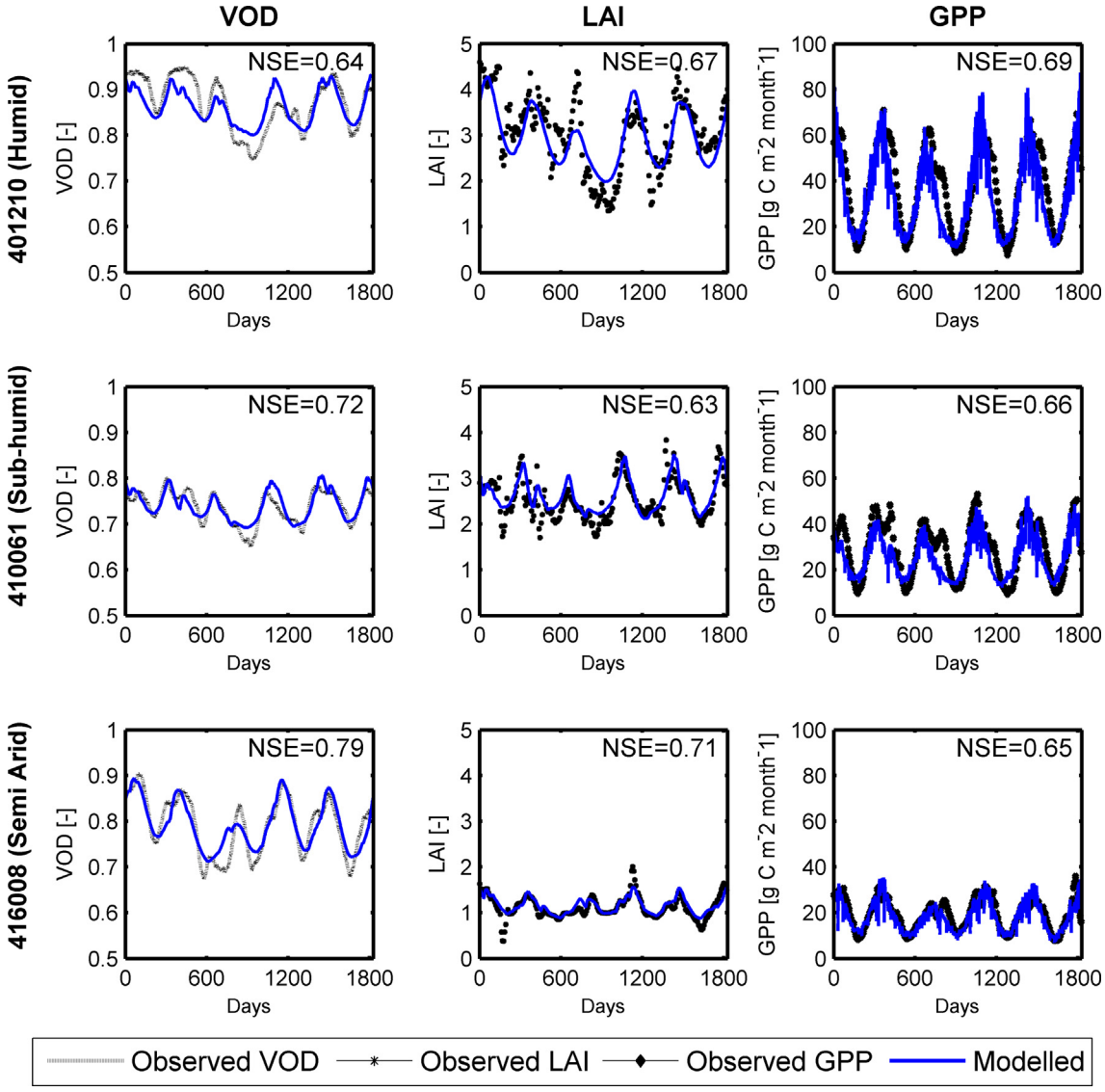


**Fig. 8.** Time series of simulated VOD, LAI and GPP for the validation period of 2001–2005 in humid, sub-humid and semi-arid catchments in comparison to observation.

ability of a multi-objective algorithm to simulate two response outputs while reasonably well simulating other vegetation attributes. In addition, our results support the contention of Vrugt et al. (2003) that a multi-objective algorithm measures the different aspects of system behaviour and can provide a set of trade-off solutions in a single simulation run.

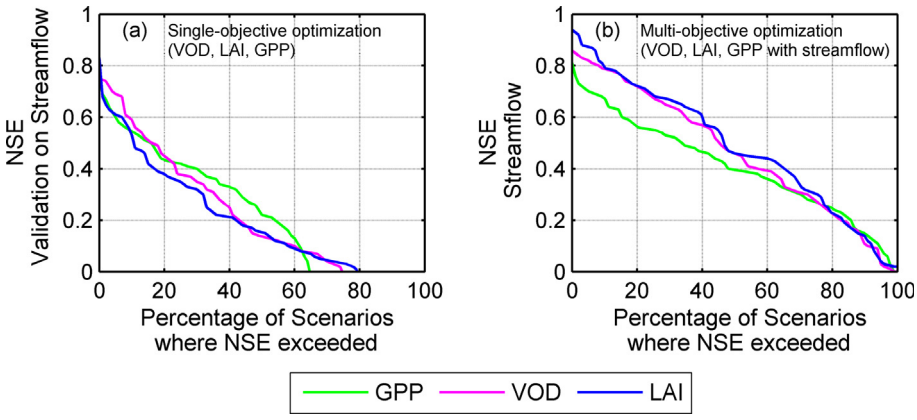


**Fig. 9.** Single-objective validation and multi-objective optimization for streamflow prediction, (a) the set of parameters obtained through single-objective calibration of GPP, VOD and LAI was applied for streamflow prediction, (b) NSE score for streamflow prediction using multi-objective optimization when applied for LAI and streamflow, VOD and streamflow, GPP and streamflow. The CDF curves are plotted only for one response output (streamflow).

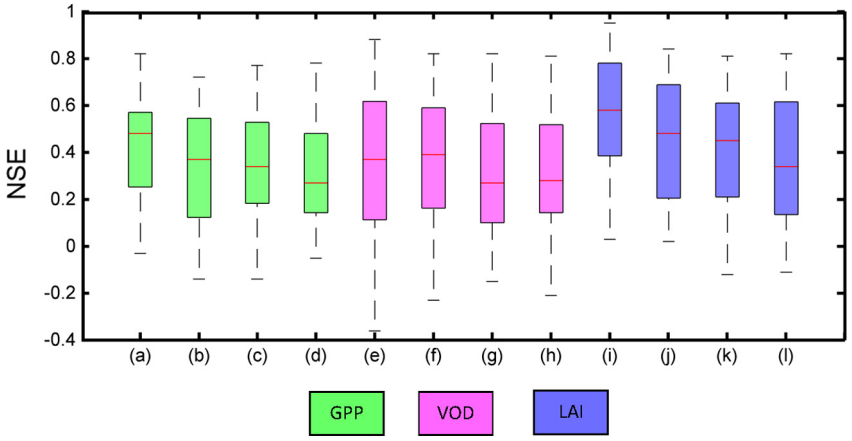


**Fig. 10.** Box plots show model validations on streamflow prediction (split sample and nearest neighbour regionalisation) when the model is calibrated simultaneously for streamflow and vegetation product (GPP, VOD and LAI). Calibration of streamflow using GPP, VOD and LAI in (a), (e) and (i); validations of same catchments for streamflow are in (b), (f) and (j), Validation on nearest neighbour catchments for scenario 1 (2001–2005) are presented in (c), (g) and (k) for streamflow with GPP, VOD and LAI and Validation on nearest neighbour catchments for scenario 2 (2006–2010) are presented in (d), (h) and (l) for streamflow with GPP, VOD and LAI.

In the light of our results we conclude that LAI would be the best indicator of ecological properties in conceptual ecohydrological modeling of the catchment and the water balance. Because variability in LAI or vegetation cover impacts evapotranspiration and runoff, it should be considered for making runoff projections based on climate change scenarios (Tesemma et al., 2015b).

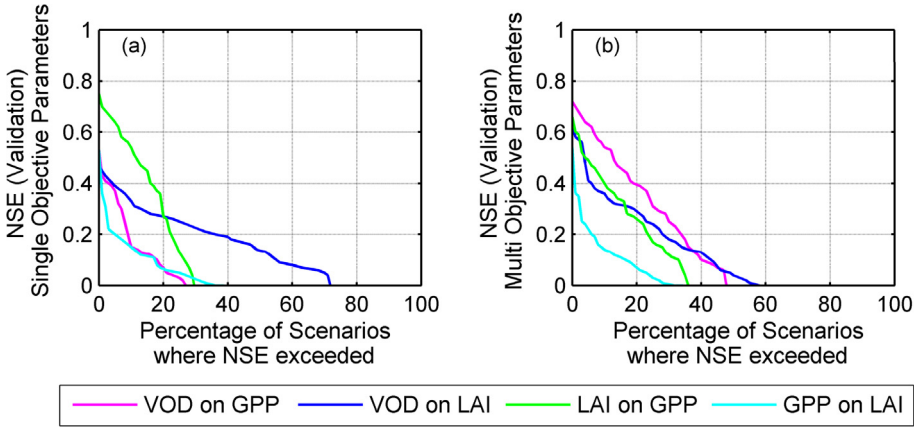


**Fig. 11.** NSE score of cross validation performed for vegetation attributes. Cross validation of (a) single-objective and (b) multi-objective calibrated parameters of VOD validated on LAI and GPP, GPP on LAI and calibrated parameters of LAI that are validated for GPP.

## 5. Discussions

### 5.1. What could explain differences in the performance of the model for different vegetation products and catchments?

Single-objective calibration and validation of EcoHydr using each product (GPP, LAI and VOD is performed to identify the best simulated product in a conceptual ecohydrological model. We found that GPP is the best simulating vegetation product in EcoHydr. However, in some catchments located in arid zones low NSE values are obtainedfor GPP simulations. The reason for this low performance is related to the GPP computation based on ET (Eq. (5), Supplementary Material) which includes both evaporation and transpiration. It is recommended to use transpiration instead of ET in catchments with sparse vegetation cover. Another reason for the poor performance is related to the use of constant WUE parameter for GPP estimation in our model (Emmerich, 2003; Istanbulluoglu et al., 2011 ).

Simulated LAI based on EcoHydr model is not as good as previously reported values by Istanbulluoglu et al. (2011) (Table 1) using the Bucket Grassland Model (BGM). Istanbulluoglu et al. (2011) showed that the BGM model captures the onset of the growing season, the timing of the peak biomass and its decay reasonably well. While EcoHydro uses the same model structure as the BGM for simulating vegetation dynamics, the scale of simulations and vegetation types are different in both studies. BGM is developed to simulate leaf biomass in grassland research plots while here it is used for simulating biomass in catchments that are mostly covered by trees. Montaldo et al. (2005) used five vegetation dynamics models with different structures and all models predicted LAI dynamics and soil water balances well in the Californian C3 grass field sites characterized by a Mediterranean climate and water-limited conditions. Therefore lower NSE values of LAI simulations in this study is a result of large and heterogeneous catchments covered by mixed species of Eucalypts and other vegetation.

The results of VOD simulations are equally good as of LAI (Fig. 3a–d).VOD is a unique vegetation product that has significant potential for use in hydrological modeling to characterize the water content in above ground biomass (canopy and wood). While VOD is mainly used for vegetation monitoring across the globe (Andela et al., 2013; Liu et al., 2011, 2013, 2015), here it is used to assess ecohydrological conceptualization. Van Dijk et al. (2013) simulated NDVI and VOD using AWRA model for agriculture drought assessment. Using VOD as an indicator of wheat crop yield showed lower yield during the drought compared to the average condition. Our model also shows that VOD is well simulated in a conceptual ecohydrological model and its coarse spatial resolution doesn't affect the results (Fig. 4a and b).

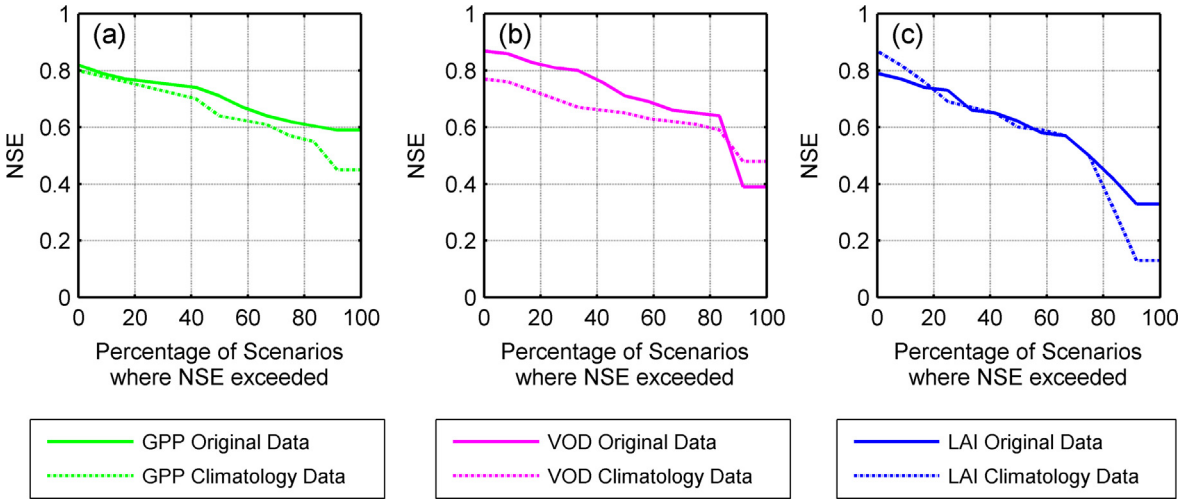


**Fig. 12.** Assessing the model performance for simulating GPP, VOD and LAI using satellite time series data versus vegetation climatology.

**Table 6**
Comparison of EcoHydr simulations for satellite-derived time series data and vegetation climatology data.

| Catchment ID | Climate zone | Scenario calibration[a] | NSE original (satellite) data calibration | | | NSE climatology data calibration | | |
|---|---|---|---|---|---|---|---|---|
| | | | GPP | VOD | LAI | GPP | VOD | LAI |
| 401210 | Humid | 1 | 0.74 | 0.86 | 0.73 | 0.70 | 0.73 | 0.76 |
| 401210 | Humid | 2 | 0.64 | 0.80 | 0.58 | 0.64 | 0.65 | 0.65 |
| 401216 | Humid | 1 | 0.77 | 0.83 | 0.65 | 0.80 | 0.77 | 0.87 |
| 401216 | Humid | 2 | 0.76 | 0.76 | 0.79 | 0.76 | 0.76 | 0.82 |
| 401220 | Sub-humid | 1 | 0.79 | 0.81 | 0.74 | 0.72 | 0.73 | 0.69 |
| 401220 | Sub-humid | 2 | 0.67 | 0.71 | 0.42 | 0.64 | 0.67 | 0.50 |
| 403224 | Sub-humid | 1 | 0.76 | 0.65 | 0.57 | 0.57 | 0.66 | 0.32 |
| 403224 | Sub-humid | 2 | 0.62 | 0.39 | 0.33 | 0.45 | 0.48 | 0.13 |
| 410024 | Sub-humid | 1 | 0.82 | 0.87 | 0.66 | 0.80 | 0.61 | 0.67 |
| 410024 | Sub-humid | 2 | 0.71 | 0.64 | 0.50 | 0.74 | 0.59 | 0.60 |
| 426533 | Semi-arid | 1 | 0.62 | 0.69 | 0.77 | 0.55 | 0.63 | 0.59 |
| 426533 | Semi-arid | 2 | 0.59 | 0.66 | 0.62 | 0.61 | 0.62 | 0.57 |

[a] Scenario 1: 2001–2005, Scenario 2: 2006–2010.

The results of grouping of the catchments on the basis of aridity show that the model is working significantly better in humid catchments for GPP, VOD and LAI. Our findings are consistent with Li and Ishidaira (2012) (Table 1). They validated the coupled ecohydrological model LPJH for simulating annual LAI against annual maximum and accumulated values of NDVI (acquired from the

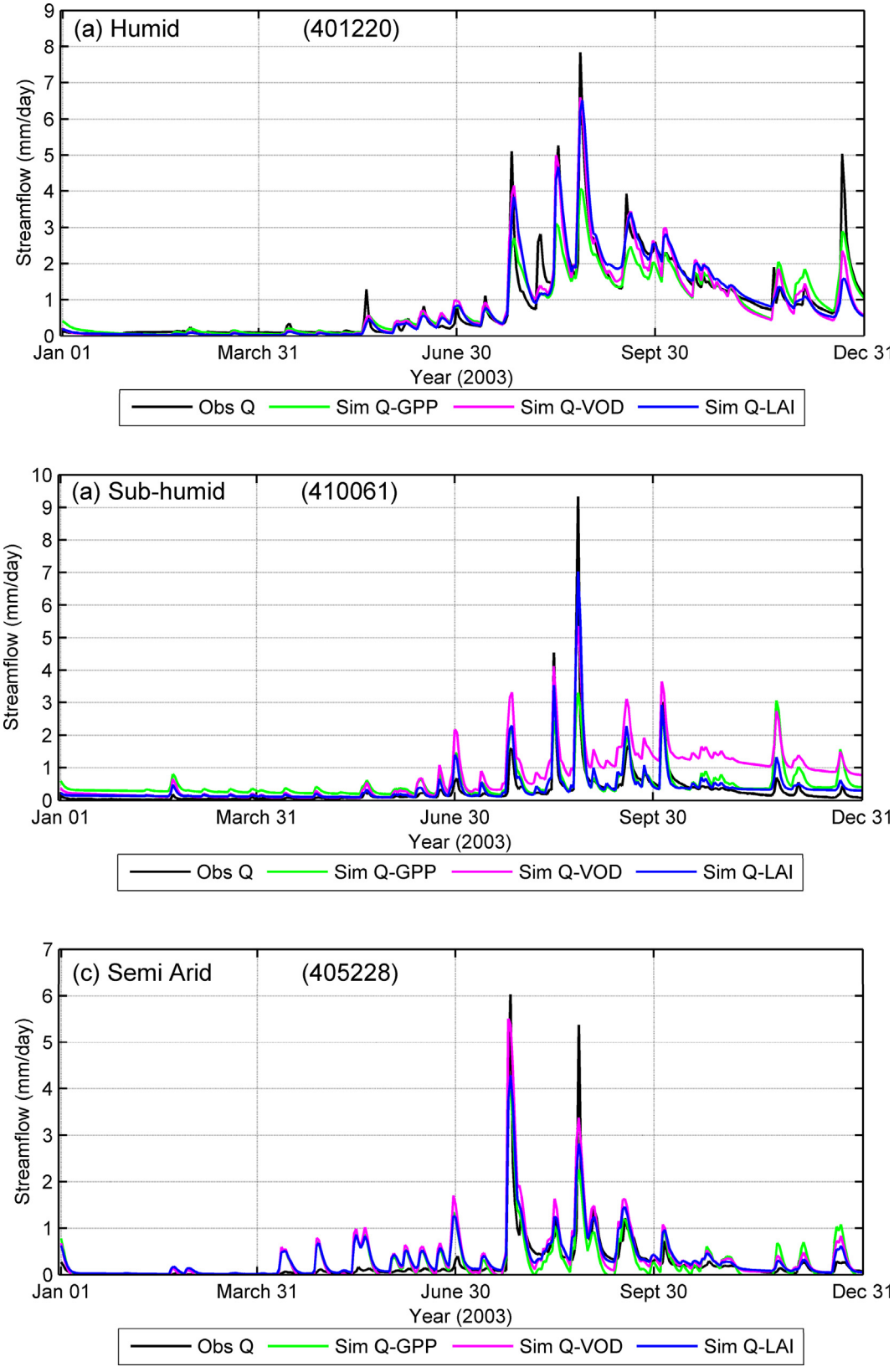


**Fig. 13.** Comparison of observed and simulated streamflow by GPP, VOD and LAI in three different catchments; (a) Humid catchment; (b) Sub-humid catchment and (c) Semi-arid catchment. Among three satellite-derived vegetation products, LAI simulates the best streamflow.

Advanced Very High Resolution Radiometer (AVHRR) sensor aboard NOAA satellites and processed by the Global Inventory Monitoring and Modeling Studies (GIMMS) at the National Aeronautics and Space Administration (NASA)) and basin averaged NDVI calculated from semi-monthly data. On the basis of a linear relationship between NDVI and LAI obtained from previous studies, their model simulated LAI reasonably well in humid and sub-humid basins while the model's performance was poor in arid and semi-arid basins due to neglecting the shrub type in plant functional types of LPJ (vegetation dynamics model of coupled LPJH model). Hence, vegetation type is a significant factor in simulating LAI in conceptual ecohydrological modeling. As stated by Pasquato et al. (2014), the MODIS dataset (LAI, EVI) can be used for ecohydrological model calibration. However, error within the remote sensing data may give rise to uncertainty in modeling vegetation attributes.

Niu et al. (2014) used a process based ecohydrological model in an experimental watershed in Arizona and selected C4 warm grasses as the vegetation type. The results showed that LAI, surface water and $CO_2$ fluxes were simulated quite well over the entire catchment. MODIS LAI is used as observed data for comparison with observed net $CO_2$ fluxes. At the seasonal and interannual scales, results showed that the modeled LAI, runoff, and soil moisture are comparable with the observations. EcoHydr is a conceptual ecohydrolgical model and despie its simple structure our results indicate the performance of the model is good in comparison with observations and seasonal dynamics of vegetation simulations are well captured by the model as shown in Fig. 8.

Our results highlighted the importance of remote sensing datasets in ecohydrological modeling across heterogenous catchments with Eucalypttrees compared to other studies targeting experimental plots and grasses. We also found that remote sensing datasets provide useful information for simultaneous calibration of two response ouputs. We identified the best vegetation product using a multi-objective algorithm for streamflow estimation. Previous research studies by Zhang et al. (2009), Van Dijk et al. (2013), Tesemma et al. (2015a and 2015b) demonstrate that incorporating LAI in hydrological models improves mean monthly and annual streamflow prediction.

### 5.2. Can vegetation climatology data provide similar results as the time series data for ecohydrologic model calibration?

To show the impact of inter-annual vegetation dynamics in conceptual ecohydrologic model calibration, we calibrated the model using the vegetation climatology data obtained from satellite time series in a sample of 6 catchments (2 humid, 2 sub-humid and 2 semi-arid). A cumulative response of all catchments is shown in Fig. 12. It is found that model performance gets affected using vegetation climatology data of GPP, LAI and VOD versus the time series data representing inter-annual variability. The results indicate that the NSE value deteriorates in sub-humid and semi-arid catchments using GPP, VOD and LAI climatology data. However, some improvements in NSE is seen when LAI climatology data is used for humid catchments. In most scenarios for humid catchments, NSE remains unchanged using GPP data while NSE becomes lower for VOD climatology data (Table 6).

### 5.3. What is the best vegetation product for streamflow prediction?

Results of multi-objective calibration experiments show that LAI is the best simulating vegetation product for streamflow estimation. As expected better streamflow simulation is obtained when both response outputs (streamflow with other vegetation attribute) are calibrated together (Fig. 9b). Vegetation exerts considerable control over catchment water balance and consequently affects the streamflow (Emanuel et al., 2010; Naseem et al., 2015; Tesemma et al., 2015a, 2015b; Thompson et al., 2011; Zhang et al., 2009). LAI is one of the physical properties of the catchment and it clearly provides improvement in streamflow prediction when its simulation is included as one of the objective functions in our multi-objective experiment. Similarly, essential parameterized components of dynamic vegetation modeling including photosynthesis, autotrophic respiration, carbon allocation, and phenology (Arora, 2002) are factors that impact evapotranspiration and interception simulation in hydrological modeling. These components are part of the EcoHydr model (Fig. 2). Moreover, LAI is a strong indicator of the vegetation cover fraction that characterizes the catchment water balance and hence affects the streamflow (Yang et al., 2009). Although spatial and temporal resolution of VOD dataset are different than LAI, VOD is reproducing streamflow as good as with LAI. VOD could potentially be one of the best vegetation products to assess the relationship between climatic variability, vegetation cover, catchment water balance and streamflow prediction due to its characteristics for measuring canopy density and vegetation water content. The model's lower performance for multi-objective calibration with GPP and streamflow is basically related to GPP being the measure of vegetation productivity at the beginning of the carbon cycle and its influence is progressively reduced by plant respiration processes.

To evaluate the streamflow simulation in a multi-objective calibration using one of the vegetation products GPP, LAI or VOD with streamflow, three catchments in humid, sub-humid and semi-arid zones are selected.

In the humid and sub-humid catchments, the model is producing reasonably good estimates of streamflow when LAI and VOD are used for multi-objective calibration with streamflow (Fig. 13a and b). In the semi-arid catchment, the best streamflow simulation is obtained by multi-objective calibration of GPP particularly during summer (December-February) and streamflow pre-

**Table 7**
Average NSE values of summer and winter seasons for streamflow.

| Catchment | Scenario | GPP | | VOD | | LAI | |
|---|---|---|---|---|---|---|---|
| | | Summer | Winter | Summer | Winter | Summer | Winter |
| 401210 | 1 | 0.49 | 0.57 | 0.54 | 0.58 | 0.54 | 0.58 |
| 401210 | 2 | 0.75 | 0.39 | 0.72 | 0.38 | 0.64 | 0.42 |
| 401216 | 1 | 0.04 | 0.09 | 0.16 | 0.11 | 0.20 | 0.11 |
| 401216 | 2 | 0.63 | 0.63 | 0.64 | 0.63 | 0.64 | 0.63 |
| 401220 | 1 | 0.53 | 0.21 | 0.53 | 0.22 | 0.53 | 0.21 |
| 401220 | 2 | 0.48 | 0.51 | 0.49 | 0.52 | 0.37 | 0.54 |
| 410061 | 1 | 0.57 | 0.44 | 0.54 | 0.66 | 0.54 | 0.33 |
| 410061 | 2 | 0.48 | 0.20 | 0.42 | 0.50 | 0.42 | 0.50 |
| 405228 | 1 | 0.50 | 0.38 | 0.66 | 0.48 | 0.66 | 0.46 |
| 405228 | 2 | 0.43 | 0.55 | 0.48 | 0.55 | 0.48 | 0.55 |

diction is worse throughout the year when VOD based calibration is used (Fig. 13c). LAI simulates streamflow the best, as indicated by higher NSE (0.73) as compared to GPP and VOD and the seasonal pattern of streamflow is well-captured by LAI. Further we computed streamflow based NSE for two seasons, i-e summer (Dec-Feb) and winter (Jun-Aug) months using results of multi-objective calibration for Scenario 1 (2001–2005). As can be seen in Table 7 there is a significant variation in the performance of the model for simulating streamflow in both seasons and results tend to be better in summer in these selected catchments.

All three remote sensing products improve streamflow simulations in different manners. The GPP is calculated using observations of vegetation at the beginning of the carbon cycle and is the primary indicator of vegetation carbon fluxes. In addition, GPP is linearly related to daily evapotranspiration through an ecosystem water use efficiency parameter [WUE, kg $CO_2$ $kg^{-1}$ $H_2O$] representing the amount of carbon gained for each unit of water lost (Williams and Albertson, 2004). Improved estimates in evapotranspiration lead to better streamflow prediction.

The potential for remote sensing data to ingest into hydrological model to improve streamflow prediction is therefore extremely valuable and could greatly improve our understanding of water balance and seasonal patterns of streamflow and vegetation dynamics.

## 6. Conclusion

In this study, single-objective optimization was performed on three satellite derived vegetation products including LAI, VOD and GPP using a verified conceptual ecohydrological model (EcoHydr). We found that GPP was the best simulating product in our model as compared to VOD and LAI when single objective optimization was performed. It wass observed that improvement in vegetation simulation was not consistent across all scenarios and catchments during the validation period due to differences in catchment climate and soil type. Our ultimate goal was identification of a satellite derived vegetation product to be a part of a conceptual ecohydrological model for better streamflow prediction. To assess this product, a multi-objective technique was implemented to obtain the best compromised solution for both output responses (vegetation and streamflow) in three cases including GPP and streamflow, VOD and streamflow and LAI and streamflow. The multi-objective optimizations of EcoHydr based on simultaneous calibration of streamflow and LAI showed the best performance for streamflow prediction in conjunction with LAI simulation. The addition of LAI dynamics in the hydrological model improved the streamflow prediction indicated by higher NSE values compared to VOD and GPP runs with streamflow. The model simulated streamflow acceptably well by taking LAI dynamics into account.

Our results illustrate that a conceptual ecohydrological model simulated vegetation products differently on the basis of the parameterization of vegetation dynamics and their role in the carbon cycle. In addition, the benefit of using multi-objective optimization for two response outputs, streamflow and LAI simultaneously, show that LAI should be part of a conceptual ecohydrological model. Future research should focus on computing the significant processes, including interception, evapotranspiration and vegetation fraction cover using observed satellite derived vegetation products to assess performance of a conceptual ecohydrological model for streamflow prediction.

## Acknowledgements

The authors acknowledge partial funding for this work from the Australian Research Council.

We thank editor (Tim R. McVicar), associate editor (Yongqiang Zhang) and three anonymous reviewers for the comments that improved this manuscript. The lead author is thankful to the Department of Education and Training, Australia for Endeavour Scholarship for funding her PhD studies at UNSW.

## Appendix A. Supplementary material

Supplementary data associated with this article can be found, in the online version, at http://dx.doi.org/10.1016/j.jhydrol.2016.10.038.

## References

Andela, N., Liu, Y., van Dijk, A., de Jeu, R., McVicar, T., 2013. Global changes in dryland vegetation dynamics (1988–2008) assessed by satellite remote sensing: comparing a new passive microwave vegetation density record with reflective greenness data. Biogeosciences 10 (10), 6657.

Ardö, J., 2015. Comparison between remote sensing and a dynamic vegetation model for estimating terrestrial primary production of Africa. Carbon Balance Manage. 10 (1), 8.

Arnold, J.G. et al., 2012. SWAT: model use, calibration, and validation. Transact. ASABE 55 (4), 1491–1508.

Arnold, S., Attinger, S., Frank, K., Hildebrandt, A., 2009. Uncertainty in parameterisation and model structure affect simulation results in coupled ecohydrological models. Hydrol. Earth Syst. Sci. 13 (10), 1789–1807.

Arora, V., 2002. Modeling vegetation as a dynamic component in soil-vegetation-atmosphere transfer schemes and hydrological models. Rev. Geophys. 40 (2), 1006.

Boyle, D.P., Gupta, H.V., Sorooshian, S., 2003. Multicriteria calibration of hydrologic models. Water Sci. Appl. 6, 185–196.

Brown, A.E., Zhang, L., McMahon, T.A., Western, A.W., Vertessy, R.A., 2005. A review of paired catchment studies for determining changes in water yield resulting from alterations in vegetation. J. Hydrol. 310 (1), 28–61.

Bréda, N.J., 2003. Ground-based measurements of leaf area index: a review of methods, instruments and current controversies. J. Exp. Bot. 54 (392), 2403–2417.

Butcher, J.C., 2008. Numerical Methods for Ordinary Differential Equations. John Wiley & Sons.

Ceccherini, G., Castelli, F., 2012. Vegetation Response to Climate, Eco-hydrological Modeling at Basin Scale in Water-limited Ecosystems, pp. 5637.

Ceola, S. et al., 2010. Comparative study of ecohydrological streamflow probability distributions. Water Resour. Res. 46 (9), W09502.

Cervarolo, G., Mendicino, G., Senatore, A., 2010. A coupled ecohydrological–three-dimensional unsaturated flow model describing energy, $H_2O$ and $CO_2$ fluxes. Ecohydrology 3 (2), 205–225.

Choler, P., Sea, W., Briggs, P., Raupach, M., Leuning, R., 2010. A simple ecohydrological model captures essentials of seasonal leaf dynamics in semi-arid tropical grasslands. Biogeosciences 7 (3), 907–920.

Crockford, R., Richardson, D., 1990. Partitioning of rainfall in a eucalypt forest and pine plantation in southeastern Australia: IV The relationship of interception and canopy storage capacity, the interception of these forests, and the effect on interception of thinning the pine plantation. Hydrol. Process. 4 (2), 169–188.

Donohue, R.J., McVicar, T., Roderick, M.L., 2009. Climate-related trends in Australian vegetation cover as inferred from satellite observations, 1981–2006. Glob. Change Biol. 15 (4), 1025–1039.

Donohue, R.J., McVicar, T.R., Roderick, M.L., 2010. Assessing the ability of potential evaporation formulations to capture the dynamics in evaporative demand within a changing climate. J. Hydrol. 386 (1), 186–197.

Donohue, R.J., Roderick, M.L., McVicar, T.R., 2012. Roots, storms and soil pores: Incorporating key ecohydrological processes into Budyko's hydrological model. J. Hydrol. 436, 35–50.

Duan, Q., Gupta, V.K., Sorooshian, S., 1993. Shuffled complex evolution approach for effective and efficient global minimization. J. Optim. Theory Appl. 76 (3), 501–521.

Duan, Q., Sorooshian, S., Gupta, V., 1992. Effective and efficient global optimization for conceptual rainfall-runoff models. Water Resour. Res. 28 (4), 1015–1031.

Ediriweera, S., Pathirana, S., Danaher, T., Nichols, D., 2014. Estimating above-ground biomass by fusion of LiDAR and multispectral data in subtropical woody plant communities in topographically complex terrain in North-eastern Australia. J. Forest. Res. 25 (4), 761–771.

Emanuel, R.E. et al., 2010. Spatial and temporal controls on watershed ecohydrology in the northern Rocky Mountains. Water Resour. Res. 46 (11).

Emmerich, W.E., 2003. Carbon dioxide fluxes in a semiarid environment with high carbonate soils. Agr. Forest Meteorol. 116 (1), 91–102.

Fenicia, F., Savenije, H.H., Matgen, P., Pfister, L., 2007. A comparison of alternative multiobjective calibration strategies for hydrological modeling. Water Resour. Res. 43 (3).

Gereta, E., Wolanski, E., Borner, M., Serneels, S., 2002. Use of an ecohydrology model to predict the impact on the Serengeti ecosystem of deforestation, irrigation and the proposed Amala Weir Water Diversion Project in Kenya. Ecohydrol. Hydrobiol. 2 (1–4), 135–142.

Glenn, E.P., Huete, A.R., Nagler, P.L., Nelson, S.G., 2008. Relationship between remotely-sensed vegetation indices, canopy attributes and plant physiological processes: what vegetation indices can and cannot tell us about the landscape. Sensors 8 (4), 2136–2160.
Heinsch, F.A. et al., 2003. GPP and NPP (MOD17A2/A3) Products NASA MODIS Land Algorithm. MOD17 User's Guide: 1–57.
Heiskanen, J., 2006. Estimating aboveground tree biomass and leaf area index in a mountain birch forest using ASTER satellite data. Int. J. Remote Sens. 27 (6), 1135–1158.
Huete, A., Didan, K., Shimabakuro, Y., Ratana, P., Saleska, S., Hutyra, L., Yang, W., Nemani, R., Myneni, R., 2006. Amazon rainforest green-up with sunlight in dry season. Geophys. Res. Lett. 33, L06405.
Hunt, M.A., Murray, K.E., Battaglia, M., Mathers, N.J., 2007. Determination of specific leaf area of some commercially useful sub-tropical hardwood species. Austral. Forest. 70 (3), 158–166.
Istanbulluoglu, E., Wang, T., Wedin, D.A., 2011. Evaluation of ecohydrologic model parsimony at local and regional scales in a semiarid grassland ecosystem. Ecohydrology 5 (1), 121–142.
Jiménez-Muñoz, J.C. et al., 2009. Comparison between fractional vegetation cover retrievals from vegetation indices and spectral mixture analysis: Case study of PROBA/CHRIS data over an agricultural area. Sensors 9 (2), 768–793.
Jin, Y. et al., 2014. Remote sensing-based biomass estimation and its spatio-temporal variations in temperate grassland, Northern China. Remote Sens. 6 (2), 1496–1513.
Jones, M.O., Jones, L.A., Kimball, J.S., McDonald, K.C., 2011. Satellite passive microwave remote sensing for monitoring global land surface phenology. Remote Sens. Environ. 115 (4), 1102–1114.
Jönsson, P., Eklundh, L., 2004. TIMESAT—a program for analyzing time-series of satellite sensor data. Comput. Geosci. 30 (8), 833–845.
Kelley, D. et al., 2013. A comprehensive benchmarking system for evaluating global vegetation models. Biogeosciences 10, 3313–3340.
Knyazikhin et al., 1998. Synergistic algorithm for estimating vegetation canopy leaf area index and fraction of absorbed photosynthetically active radiation from MODIS and MISR data. J. Geophys. Res. 103, 32257–32276.
Küppers, M., Küppers, B.I., Neales, T.F., Swan, A.G., 1992. Leaf gas exchange characteristics, daily carbon and water balances of the host/mistletoe pair Eucalyptus behriana F. Muell. and Amyema miquelii (Lehm. ex Miq.) Tiegh. at permanently low plant water status in the field. Trees 7 (1), 1–7.
Laio, F., Porporato, A., Ridolfi, L., Rodriguez-Iturbe, I., 2001. Plants in water-controlled ecosystems: active role in hydrologic processes and response to water stress: II. Probabilistic soil moisture dynamics. Adv. Water Resour. 24 (7), 707–723.
Li, Q., Ishidaira, H., 2012. Development of a biosphere hydrological model considering vegetation dynamics and its evaluation at basin scale under climate change. J. Hydrol. 412, 3–13.
Liu, Y. et al., 2010. Influence of cracking clays on satellite estimated and model simulated soil moisture. Hydrol. Earth Syst. Sci. 14 (6), 979–990.
Liu, Y.Y., de Jeu, R.A., McCabe, M.F., Evans, J.P., van Dijk, A.I., 2011. Global long-term passive microwave satellite-based retrievals of vegetation optical depth. Geophys. Res. Lett. 38 (18).
Liu, Y.Y., Dijk, A.I., McCabe, M.F., Evans, J.P., Jeu, R.A., 2013. Global vegetation biomass change (1988–2008) and attribution to environmental and human drivers. Glob. Ecol. Biogeogr. 22 (6), 692–705.
Liu, Y.Y. et al., 2015. Recent reversal in loss of global terrestrial biomass. Nature Clim. Change 5, 470–474. http://dx.doi.org/10.1038/nclimate2581.
Liu, Y.Y., van Dijk, A.I., de Jeu, R.A., Holmes, T.R., 2009. An analysis of spatiotemporal variations of soil and vegetation moisture from a 29-year satellite-derived data set over mainland Australia. Water Resour. Res. 45 (7).
McVicar, T.R. et al., 2012. Global review and synthesis of trends in observed terrestrial near-surface wind speeds: implications for evaporation. J. Hydrol. 416, 182–205.
Meesters, A.G.C.A., De Jeu, R., Owe, M., 2005. Analytical derivation of the vegetation optical depth from the microwave polarization difference index. IEEE Geosci. Remote Sens. Lett. 2 (2), 121–123. http://dx.doi.org/10.1109/LGRS.2005.843983.
Middleton, N., Thomas, D., 1997. World Atlas of Desertification. Arnold, Hodder Headline, PLC.
Miller, G.R. et al., 2012. Understanding ecohydrological connectivity in savannas: a system dynamics modelling approach. Ecohydrology 5 (2), 200–220.
Mokany, K., Raison, R., Prokushkin, A.S., 2006. Critical analysis of root: shoot ratios in terrestrial biomes. Glob. Change Biol. 12 (1), 84–96.
Montaldo, N., Rondena, R., Albertson, J.D., Mancini, M., 2005. Parsimonious modeling of vegetation dynamics for ecohydrologic studies of water-limited ecosystems. Water Resour. Res. 41 (10), W10416.
Mourad, M., Bertrand-Krajewski, J.-L., Chebbo, G., 2005. Calibration and validation of multiple regression models for stormwater quality prediction: data partitioning, effect of dataset size and characteristics. Water Sci. Technol. 52 (3), 45–52.
Naseem, B., Ajami, H., Cordery, I., Sharma, A., 2015. A multi-objective assessment of alternate conceptual ecohydrological models. J. Hydrol. 529, 1221–1234.
Nash, J., Sutcliffe, J., 1970. River flow forecasting through conceptual models part I—a discussion of principles. J. Hydrol. 10 (3), 282–290.
Newman, B.D. et al., 2006. Ecohydrology of water-limited environments: A scientific vision. Water Resour. Res. 42 (6).
Niu, G.Y. et al., 2014. An integrated modelling framework of catchment-scale ecohydrological processes: 2. The role of water subsidy by overland flow on vegetation dynamics in a semi-arid catchment. Ecohydrology 7 (2), 815–827.
Owe, M., De Jeu, R., Walker, J., 2001. A methodology for surface soil moisture and vegetation optical depth retrieval using the microwave polarization difference index. IEEE Trans. Geosci. Remote Sens. 39 (8), 1643–1654.
Owe, M., De Jeu, R., Holmes, T., 2008. Multisensor historical climatology of satellite-derived global land surface moisture. J. Geophys. Res. 113, F01002. http://dx.doi.org/10.1029/2007JF000769.
Pasquato, M., Medici, C., Friend, A.D., Francés, F., 2014. Comparing two approaches for parsimonious vegetation modelling in semiarid regions using satellite data. Ecohydrology 8, 1024–1036.
Prentice, I.C., et al., 2007. Dynamic Global Vegetation Modeling: Quantifying Terrestrial Ecosystem Responses to Large-scale Environmental Change, Terrestrial Ecosystems in a Changing World. Springer, pp. 175–192.
Pumo, D., Viola, F., Noto, L., 2008. Ecohydrology in Mediterranean areas: a numerical model to describe growing seasons out of phase with precipitations. Hydrol. Earth Syst. Sci. Discuss. 12 (1), 303–316.
Quevedo, D., Francés, F., 2008. A conceptual dynamic vegetation-soil model for arid and semiarid zones. Hydrol. Earth Syst. Sci. 12 (5), 1175–1187.
Rodriguez-Iturbe, I., 2000. Ecohydrology: a hydrologic perspective of climate-soil-vegetation dynamics. Water Resour. Res. 36 (1), 3–9.
Ruiz-Pérez, G., González-Sanchis, M., Del Campo, A., Francés, F., 2016. Can a parsimonious model implemented with satellite data be used for modelling the vegetation dynamics and water cycle in water-controlled environments? Ecol. Model. 324, 45–53.
Raupach, MR., Briggs, PR., Haverd, V., King, EA., Paget, M., Trudinger, CM., 2009. Australian Water Availability Project (AWAP): CSIRO Marine and Atmospheric Research Component: Final Report for Phase 3. CAWCR Technical Report No. 013. pp. 67.
Savic, D., 2002. Single-objective vs. multiobjective optimisation for integrated decision support. Integr. Assess. Dec. Support 1, 7–12.
Schymanski, S., Sivapalan, M., Roderick, M., Hutley, L., Beringer, J., 2009. An optimality-based model of the dynamic feedbacks between natural vegetation and the water balance. Water Resour. Res. 45 (1), W01412.
Schulze, E.D., Turner, N.C., Nicolle, D., Schumacher, J., 2006. Leaf and wood carbon isotope ratios, specific leaf areas and wood growth of Eucalyptus species across a rainfall gradient in Australia. Tree Physiol. 26 (4), 479–492.
Sitch, S. et al., 2003. Evaluation of ecosystem dynamics, plant geography and terrestrial carbon cycling in the LPJ dynamic global vegetation model. Glob. Change Biol. 9 (2), 161–185.
Smith, T., Sharma, A., Marshall, L., Mehrotra, R., Sisson, S., 2010. Development of a formal likelihood function for improved Bayesian inference of ephemeral catchments. Water Resour. Res. 46. http://dx.doi.org/10.1029/2010WR009514.
Smith, T., Marshall, L., Sharma, A., 2015. Modeling residual hydrologic errors with Bayesian inference. J. Hydrol. 528, 29–37.
Sur, C., Choi, M., 2013. Evaluating ecohydrological impacts of vegetation activities on climatological perspectives using MODIS gross primary productivity and evapotranspiration products at Korean Regional Flux Network Site. Remote Sens. 5 (5), 2534–2553.
Szczypta, C. et al., 2014. Suitability of modelled and remotely sensed essential climate variables for monitoring Euro-Mediterranean droughts. Geosci. Model Develop. 7 (3), 931–946.
Tesemma, Z., Wei, Y., Peel, M., Western, A., 2015a. The effect of year-to-year variability of leaf area index on Variable Infiltration Capacity model performance and simulation of runoff. Adv. Water Resour. 83, 310–322.
Tesemma, Z., Wei, Y., Peel, M., Western, A., 2015b. Including the dynamic relationship between climatic variables and leaf area index in a hydrological model to improve streamflow prediction under a changing climate. Hydrol. Earth Syst. Sci. 19 (6), 2821–2836.
Thompson, S.E., Harman, C.J., Troch, P.A., Brooks, P.D., Sivapalan, M., 2011. Spatial scale dependence of ecohydrologically mediated water balance partitioning: a synthesis framework for catchment ecohydrology. Water Resour. Res. 47 (10).
VanDijk, A.I. et al., 2013. The Millennium Drought in southeast Australia (2001–2009): natural and human causes and implications for water resources, ecosystems, economy, and society. Water Resour. Res. 49 (2), 1040–1057.
Viola, F., Pumo, D., Noto, L., 2013. EHSM: a conceptual ecohydrological model for daily streamflow simulation. Hydrol. Process. 28, 3361–3372.
Vrugt, J.A., Gupta, H.V., Bastidas, L.A., Bouten, W., Sorooshian, S., 2003. Effective and efficient algorithm for multiobjective optimization of hydrologic models. Water Resour. Res. 39. http://dx.doi.org/10.1029/2002WR001746.
Wagener, T. et al., 1999. A framework for development and application of hydrological models. Hydrol. Earth Syst. Sci. 5 (1), 13–26.
Wegehenkel, M., 2009. Modeling of vegetation dynamics in hydrological models for the assessment of the effects of climate change on evapotranspiration and groundwater recharge. Adv. Geosci. 21, 109–115.
Wei, X., 2010. Biomass estimation: a remote sensing approach. Geogr. Compass 4 (11), 1635–1647.
Williams, C.A., Albertson, J.D., 2004. Soil moisture controls on canopy-scale water and carbon fluxes in an African savanna. Water Resour. Res. 40 (9), W09302.
Williams, C.A., Albertson, J.D., 2005. Contrasting short-and long-timescale effects of vegetation dynamics on water and carbon fluxes in water-limited ecosystems. Water Resour. Res. 41 (6), W06005.
Woodward, F., Lomas, M., 2004. Vegetation dynamics–simulating responses to climatic change. Biol. Rev. 79 (03), 643–670.

Xu, X., Yang, D., Sivapalan, M., 2012. Assessing the impact of climate variability on catchment water balance and vegetation cover. Hydrol. Earth Syst. Sci. 16 (1), 43–58.
Yang, D. et al., 2009. Impact of vegetation coverage on regional water balance in the nonhumid regions of China. Water Resour. Res. 45 (7).
Yapo, P.O., Gupta, H.V., Sorooshian, S., 1998. Multi-objective global optimization for hydrologic models. J. Hydrol. 204 (1), 83–97.
Yu, G. et al., 2008. Water-use efficiency of forest ecosystems in eastern China and its relations to climatic variables. New Phytol. 177 (4), 927–937.
Zhang, L., Dawes, W., Walker, G., 2001. Response of mean annual evapotranspiration to vegetation changes at catchment scale. Water Resour. Res. 37 (3), 701–708.
Zhang, Y., Chiew, F.H., Zhang, L., Li, H., 2009. Use of remotely sensed actual evapotranspiration to improve rainfall-runoff modeling in Southeast Australia. J. Hydrometeorol. 10 (4), 969–980.
Zhang, Y., Wegehenkel, M., 2006. Integration of MODIS data into a simple model for the spatial distributed simulation of soil water content and evapotranspiration. Remote Sens. Environ. 104 (4), 393–408.
Zhao, F., Zhang, L., Xu, Z., Scott, D.F., 2010. Evaluation of methods for estimating the effects of vegetation change and climate variability on streamflow. Water Resour. Res. 46 (3).